SUPPORTING INFORMATION

Influence of ancillary ligands on the formation and functionality of oxovanadium(V) metallosupramolecular assemblies: advanced computational and catalytic analysis

Edi Topić,[a] Josipa Sarjanović,[a] Danijela Musija,[b] Mirna Mandarić,[a] Andrea Cocut,[a] Tomica Hrenar,[a] Dominique Agustin,[c,d] Jana Pisk,*[a] and Višnja Vrdoljak*[a]

Table of Contents

[a] *University of Zagreb, Faculty of Science, Department of Chemistry, Horvatovac 102a, 10000 Zagreb, Croatia; E-mail: visnja.vrdoljak@chem.pmf.hr*

[b] *University of Zagreb, School of Medicine, Department of Chemistry and Biochemistry, Šalata 3, 10000 Zagreb, Croatia.*

[c] *LCC-CNRS (Laboratoire de Chimie de Coordination), 205 Route de Narbonne, BP44099, CEDEX 4, 31077 Toulouse, France*

[d] *Department of Chemistry, IUT Paul Sabatier, Université Paul Sabatier, University of Toulouse, Av. G. Pompidou, CS20258, 81104 Castres, France*

1. Characterization of compounds

Elemental analyses (C, H, and N) were performed by the Analytical Services Laboratory of Rudjer Bošković Institute, Zagreb.

Powder X-ray diffraction (PXRD) data for qualitative phase analysis were collected on a Malvern Panalytical Aeris diffractometer in the Bragg-Brentano geometry or Malvern-Panalytical Empyrean X-ray diffractometer using CuK_α radiation (λ = 1.5406 Å). Powder patterns were collected at room temperature in the region between 5° and 40° (2ϑ). The data were collected and visualized using the Malvern Panalytical HighScore Software Suite.[1]

Single crystal diffraction (SCXRD)

High-quality single crystals were grown in a way described in the manuscript. Diffracted intensities were collected on i) Rigaku XtaLAB Synergy-S diffractometer equipped with Dualflex source (CuKα radiation, λ = 1.54184 Å), and HyPix detector using ω-scans, and ii) for **1** and **6·0.5H$_2$O·0.5CH$_3$OH** Oxford Diffraction Sapphire3 diffractometer equipped with Mo Kα source. The crystals were kept at 170 K during data collection, except for **1**, **6·0.5H$_2$O·0.5CH$_3$OH** and **3**, which were measured at RT. Data were prepared using the CrysAlis program package.[2] The structures were solved with dual space methods using SHELXT.[3] The refinement procedure by full-matrix least-squares methods based on F^2 values against all reflections included anisotropic displacement parameters for all non-H atoms. Hydrogen atoms bound to carbon atoms were placed in geometrically idealized positions and refined using the riding model with U_{iso} = 1.2U_{eq} of the connected carbon atom or as ideal CH_3 groups with U_{iso} = 1.5U_{eq}. Hydrogen atoms attached to heteroatoms were located in the difference Fourier maps at the final stages of the refinement procedure. All refinements were performed using SHELXL.[4] The SHELX programs operated within the Olex2 suite.[5] Geometrical calculations and molecular graphics were done with Platon[6] and Mercury.[7] CCDC 2367618-2367624 contain the supplementary crystallographic data for this paper. These data can be obtained free of charge via http://www.ccdc.cam.ac.uk/conts/retrieving.html (or from the Cambridge Crystallographic Data Centre, 12, Union Road, Cambridge CB2 1EZ, UK; fax: +44 1223 336033).

UV-Vis spectroscopy

The UV-Vis measurements were performed on Varian Cary Bio 100 spectrophotometer using 1-cm quartz cuvettes. The UV-Vis spectra of H_2VIH and complexes **1**–**8** were recorded in both methanol and acetonitrile at room temperature (20 °C). The low solubility of the compounds was observed in both solvents. To prepare the solutions with 15-60 μmol dm^{-3} concentrations, the compounds were dissolved for 10-60 min with applied ultrasound and mild heating. The progress of the reaction of NH_4VO_3 and H_2VIH in methanol was monitored at room temperature (20 °C). The initial reactant concentrations were 4.0×10^{-5} mol dm^{-3}.

Nuclear magnetic resonance spectra (^{1}H, APT, gHMQC and gHMBC NMR) were acquired on a Bruker Avance 600 NMR spectrometer using a C/H dual 5 mm probe and z-gradient accessories at 298K in CD_3OD or $CDCl_3$ and TMS as the internal standard.

Attenuated Total Reflectance Infrared spectra (ATR-IR) in the range 4000-450 cm^{-1} were obtained on a Perkin Elmer Spectrum One spectrometer.

Differential scanning calorimetry (DSC) method was used for getting information about the purity of hydrazone. Measurements were performed under the nitrogen stream (10 mL min^{-1}) on the TA Discovery DSC 25 instrument in the temperature range from 25 to 400 °C using Tzero aluminium pans and lids. Heating rates of 10 K min^{-1} were used for all investigations. The results were evaluated using the TA Instruments Trios (v5.1.1.46572).

Thermogravimetric analyses (TGA) were performed on a Mettler-Toledo TG/DSC 3+ Stare System thermobalance using alumina crucibles under an oxygen atmosphere in the temperature range from 25 to 600 °C. All experiments were recorded with a heating rate of 5 °C min^{-1} in a dynamic atmosphere with a flow rate of 10 mL min^{-1}. The results of TGA and experiments were evaluated using the Mettler STARe software.

Fourier Transform Infrared spectra (FTIR) of the gaseous products evolved during thermal decomposition of the complexes were recorded with the use of the thermobalance coupled online with the Nicolet iS50 FT-IR spectrometer (Thermo Scientific) by a transfer line heated at 200 °C. FTIR spectra were recorded in the range of 4000–400 cm^{-1} with a resolution of 4 cm^{-1}.

Catalytic investigation

The catalytic reactions considering cyclooctene epoxidation were followed by GC techniques on an Agilent 6890A chromatograph (Agilent Technologies, Santa Clara, CA, USA) equipped with an FID detector and CP7495 column (25 m × 0.25 mm × 0.12 µm). The GC parameters were quantified using authentic samples of the reactants and products. The conversion of cyclooctene and formation of the corresponding epoxide were calculated from calibration curves using authentic samples of the studied species relative to acetophenone as an internal standard (r^2 = 0.999). The catalytic reactions considering benzyl alcohol oxidation were followed by GC techniques on an Agilent 8860 chromatograph (Agilent Technologies, Santa Clara, CA, USA) equipped with an FID detector and HP-5 capillary column (30 m × 0.32 mm × 0.25 µm). The GC parameters were quantified using authentic samples of the reactants and products. The conversion of benzyl alcohol and formation of the corresponding aldehyde were calculated from calibration curves using authentic samples of the studied species relative to biphenyl as an internal standard (r^2 = 0.999).

1.1. PXRD

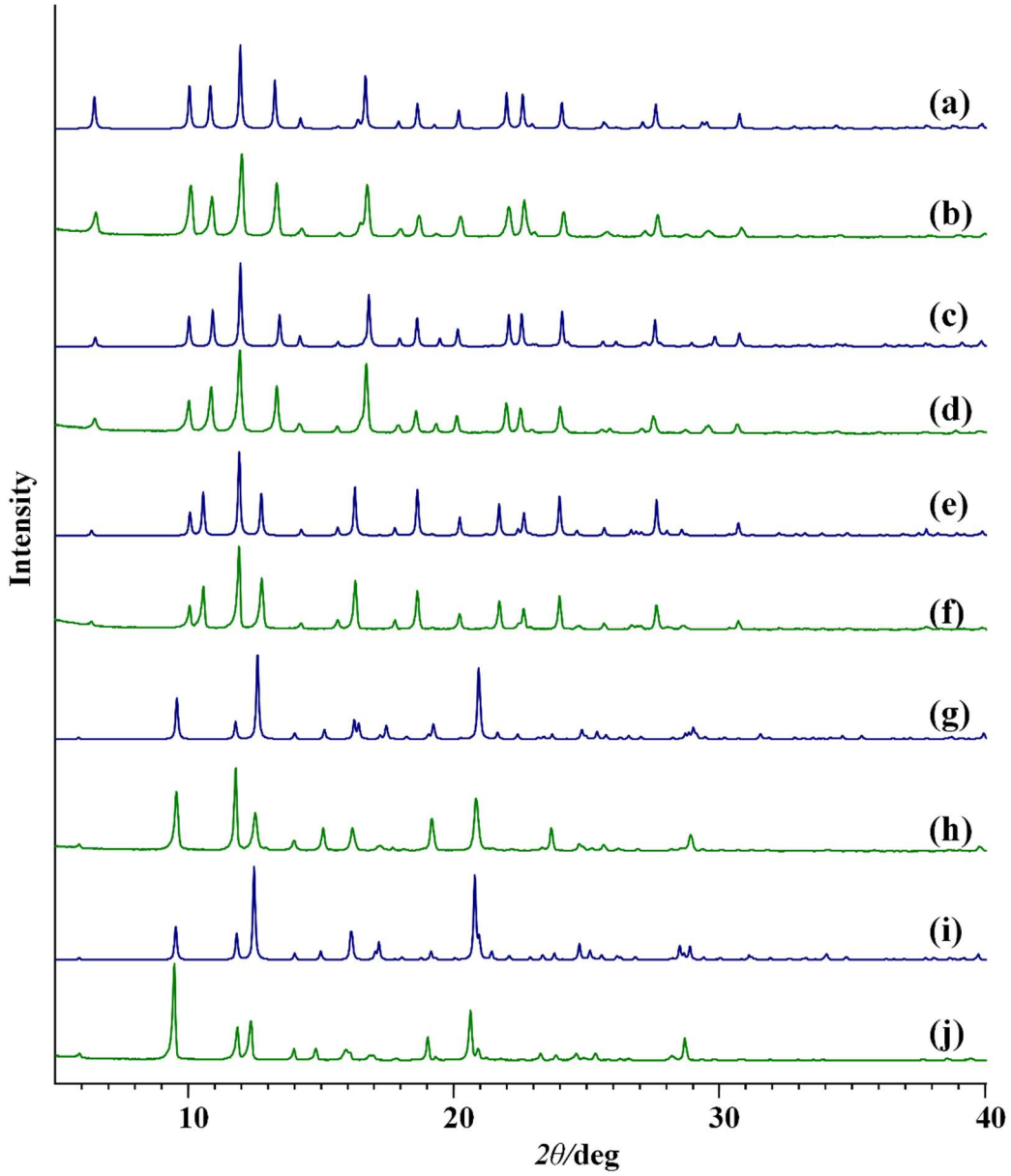

Fig. S1 PXRD patterns of the metallosupramolecular compounds: (a and b) **1**, (c and d) **2**, (e and f) **3**, (g and h) **4**, and (i and j) **5**. The green lines indicate patterns obtained by powder diffraction, while the blue lines indicate patterns calculated from the X-ray single-crystal structures of the corresponding compounds.

1.2. SCXRD

Table S1. Experimental and crystallographic data for tetranuclear complexes **1**, **2** and **3**.

Identifier	**1**	**2**	**3**
Empirical formula	$C_{60}H_{56}N_{12}O_{20}V_4$	$C_{64}H_{64}N_{12}O_{20}V_4$	$C_{68}H_{72}N_{12}O_{20}V_4$
M_r	1468.92	1525.03	1518.12
T/K	293(2)	173.16(10)	293(2)
Crystal system	tetragonal, red irregular	tetragonal, red block	tetragonal, brown block
Space group	$I\,4_1/a$	$I\,4_1/a$	$I\,4_1/a$
a/Å	17.5925(4)	17.6211(4)	17.5584(2)
b/Å	17.5925(4)	17.6211(4)	17.5584(2)
c/Å	21.6260(9)	21.2898(9)	22.6538(5)
α/°	90	90	90
β/°	90	90	90
γ/°	90	90	90
V/Å^3	6693.2(4)	6610.5(4)	6984.1(2)
Z	4	4	4
ρ_{calc}/g cm^{-3}	1.458	1.532	1.504
μ/mm^{-1}	0.622	5.322	5.058
F(000)	3008	3136	3264
Crystal size/mm^3	0.12×0.10×0.10	0.19×0.15×0.14	0.15×0.1×0.06
Radiation	MoKα (λ = 0.71073Å)	CuKα (λ = 1.54184Å)	CuKα (λ = 1.54184Å)
2Θ range/°	8.564 to 54.986	6.512 to 155.744	6.368 to 154.662
Index ranges	$-22 \le h \le 18$, $-22 \le k \le 22$, $-26 \le l \le 28$	$-22 \le h \le 12$, $-22 \le k \le 19$, $-26 \le l \le 22$	$-21 \le h \le 21$, $-22 \le k \le 21$, $-26 \le l \le 27$
Reflections collected	34740	12917	14473
Independent reflections	3830 [R_{int} = 5.29%, R_{sigma} = 3.18 %]	3441 [R_{int} = 5.27%, R_{sigma} = 5.23 %]	3531 [R_{int} = 4.33%, R_{sigma} = 5.49 %]
Data/restraints/parameters	3830/-/219	3437/-/228	3531/-/237
g_1, g_2 in w[a]	0.0623, 6.9113	0.0531, 16.2961	0.0951, 4.6355
Goodness–of–fit on F^2, S[b]	1.024	1.131	1.042
Final R and wR[c] values [$I \ge 2\sigma(I)$]	R_1 = 4.80%, wR_2 = 12.08%	R_1 = 4.68%, wR_2 = 12.33%	R_1 = 5.31%, wR_2 = 14.93%
Final R and wR[c] values [all data]	R_1 = 7.01%, wR_2 = 13.21%	R_1 = 5.58%, wR_2 = 13.52%	R_1 = 6.46%, wR_2 = 15.85%
Largest diff. peak/hole / e Å^{-3}	0.590/–0.297	0.382/–0.514	0.795/–0.275

[a] $w = 1/[\sigma F_o^2 + (g_1P)^2 + g_2P]$ where $P = (F_o^2 + 2F_c^2)/3$
[b] $S = \{\Sigma[w(F_o^2 - F_c^2)2]/(N_r - N_p)\}^{1/2}$ where N_r = number of independent reflections, N_p = number of refined parameters.
[c] $R = \Sigma||F_o| - |F_c|/\Sigma|F_o|$; $wR = \{\Sigma[w(F_o^2 - F_c^2)2]/\Sigma[w(F_o^2)2]\}^{1/2}$

Table S2. Experimental and crystallographic data for coordination polymers **4** and **5**

Identifier	**4**	**5**
Empirical formula	$C_{18}H_{19}N_3O_5V$	$C_{19}H_{22}N_3O_5V$
M_r	408.30	423.33
T/K	169.99(10)	170.00(10)
Crystal system	orthorhombic, brown block	orthorhombic, brown needle
Space group	$P\,c\,a\,2_1$	$P\,c\,a\,2_1$
a/Å	11.7033(9)	11.8119(5)
b/Å	15.0094(10)	14.9558(6)
c/Å	10.7908(8)	10.9912(6)
α/°	90	90
β/°	90	90
γ/°	90	90
V/Å^3	1895.5(2)	1941.67(16)
Z	4	4
ρ_{calc}/g cm^{-3}	1.431	1.448
μ/mm^{-1}	4.678	4.586
F(000)	844	880
Crystal size/mm^3	0.11×0.06×0.05	0.17×0.05×0.03
Radiation	CuKα (λ = 1.54184Å)	CuKα (λ = 1.54184Å)
2Θ range/°	5.888 to 154.942	5.91 to 156.316
Index ranges	$-13 \le h \le 14$, $-14 \le k \le 18$, $-8 \le l \le 13$	$-14 \le h \le 13$, $-18 \le k \le 18$, $-13 \le l \le 13$
Reflections collected	7936	8648
Independent reflections	2792 [R_{int} = 5.37%, R_{sigma} = 5.25 %]	3226 [R_{int} = 7.63%, R_{sigma} = 6.94 %]
Data/restraints/parameters	2792/49/268	3226/48/277
g_1, g_2 in w[a]	0.0756, 1.5163	0.0905, 1.5530
Goodness–of–fit on F^2, S[b]	1.090	1.149
Final R and wR[c] values [$I \ge 2\sigma(I)$]	R_1 = 4.99%, wR_2 = 13.23%	R_1 = 5.41%, wR_2 = 14.42%
Final R and wR[c] values [all data]	R_1 = 6.00%, wR_2 = 14.24%	R_1 = 6.88%, wR_2 = 17.93%
Largest diff. peak/hole / e Å^{-3}	0.542/–0.497	0.540/–0.640

[a] $w = 1/[\sigma F_o^2 + (g_1P)^2 + g_2P]$ where $P = (F_o^2 + 2F_c^2)/3$

[b] $S = \{\Sigma[w(F_o^2 - F_c^2)2]/(N_r - N_p)\}^{1/2}$ where N_r = number of independent reflections, N_p = number of refined parameters.

[c] $R = \Sigma||F_o| - |F_c||/\Sigma|F_o|$; $wR = \{\Sigma[w(F_o^2 - F_c^2)2]/\Sigma[w(F_o^2)2]\}^{1/2}$

Table S3. Experimental and crystallographic data for **6·2H$_2$O** and **6·0.5H$_2$O·0.5CH$_3$OH**

Identifier	**6·2H$_2$O**	**6·0.5H$_2$O·0.5CH$_3$OH**
Empirical formula	$C_{14}H_{15}N_3O_7V$	$C_{29}H_{29}N_6O_{12}V_2$
M_r	388.23	755.46
T/K	169.99(10)	293(2)
Crystal system	triclinic, orange irregular	monoclinic, orange block
Space group	$P\,\bar{1}$	$C\,1\,c\,1$
a/Å	7.2890(3)	15.4904(9)
b/Å	10.4109(5)	30.9857(12)
c/Å	10.5800(4)	14.0729(10)
α/°	107.183(4)	90
β/°	97.280(3)	107.513(7)
γ/°	91.817(4)	90
V/Å^3	758.82(6)	6441.6(7)
Z	2	8
ρ_{calc}/g cm^{-3}	1.699	1.455
μ/mm^{-1}	5.908	0.643
F(000)	398	2872
Crystal size/mm^3	0.132×0.069×0.031	0.74×0.34×0.25
Radiation	CuKα (λ = 1.54184Å)	MoKα (λ = 0.71073Å)
2Θ range/°	8.838 to 155.51	8.376 to 53.0
Index ranges	$-9 \le h \le 8$, $-13 \le k \le 13$, $-13 \le l \le 13$	$-19 \le h \le 19$, $-38 \le k \le 28$, $-17 \le l \le 17$
Reflections collected	11559	14553
Independent reflections	3175 [R_{int} = 3.9%, R_{sigma} = 3.61 %]	10650 [R_{int} = 6.43%, R_{sigma} = 3.49 %]
Data/restraints/parameters	3175/-/230	10650/-/837
g_1, g_2 in w[a]	0.1286, 0.1069	0.0265, 0
Goodness–of–fit on F^2, S[b]	1.085	0.970
Final R and wR[c] values [$I \ge 2\sigma(I)$]	R_1 = 5.92%, wR_2 = 17.75%	R_1 = 4.69%, wR_2 = 8.3%
Final R and wR[c] values [all data]	R_1 = 6.27%, wR_2 = 18.20%	R_1 = 6.46%, wR_2 = 9.11%
Largest diff. peak/hole / e Å^{-3}	1.035/–0.596	0.320/–0.269

[a] $w = 1/[\sigma F_o^2 + (g_1P)^2 + g_2P]$ where $P = (F_o^2 + 2F_c^2)/3$
[b] $S = \{\Sigma[w(F_o^2 - F_c^2)2]/(N_r - N_p)\}^{1/2}$ where N_r = number of independent reflections, N_p = number of refined parameters.
[c] $R = \Sigma||F_o| - |F_c||/\Sigma|F_o|$; $wR = \{\Sigma[w(F_o^2 - F_c^2)2]/\Sigma[w(F_o^2)2]\}^{1/2}$

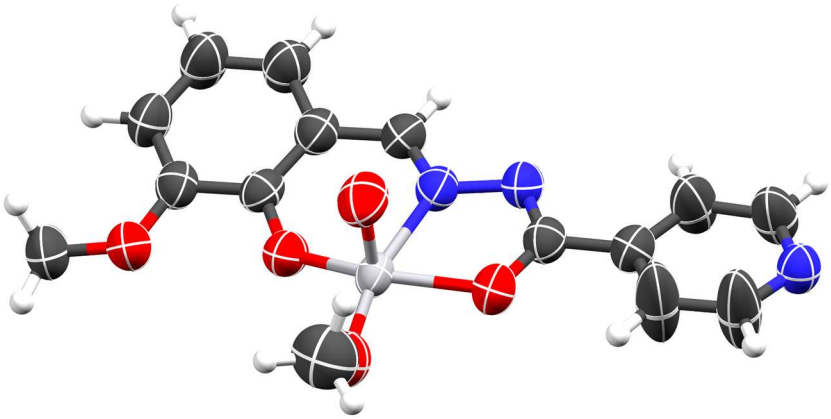

(a)

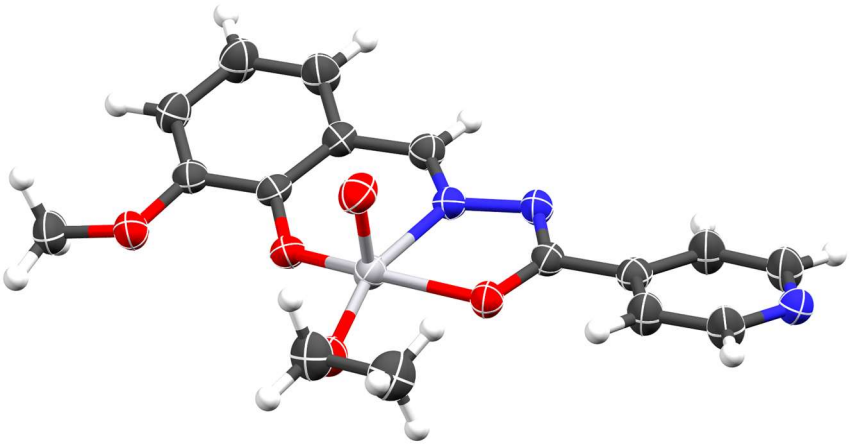

(b)

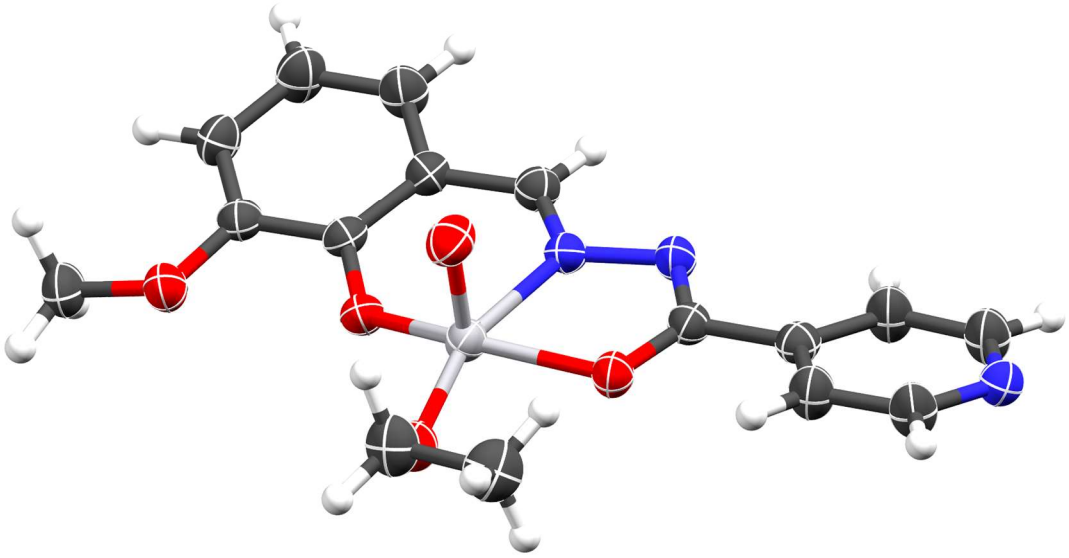

(c)

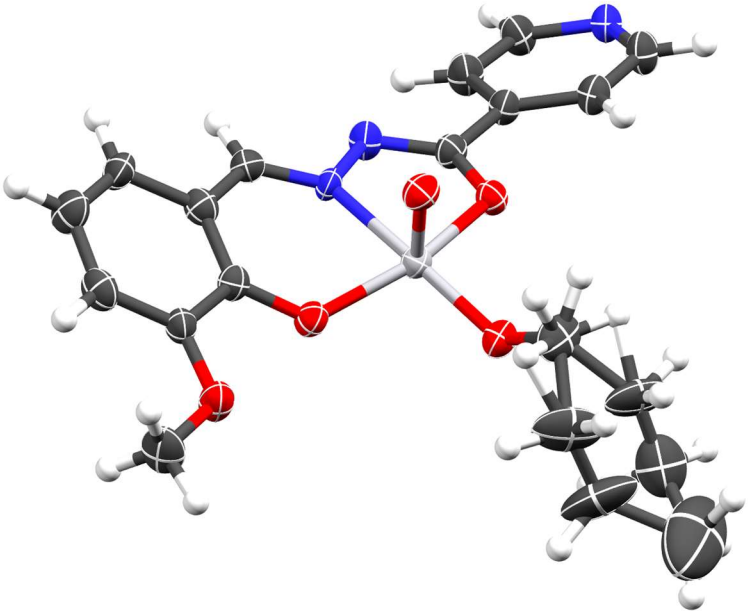

(d)

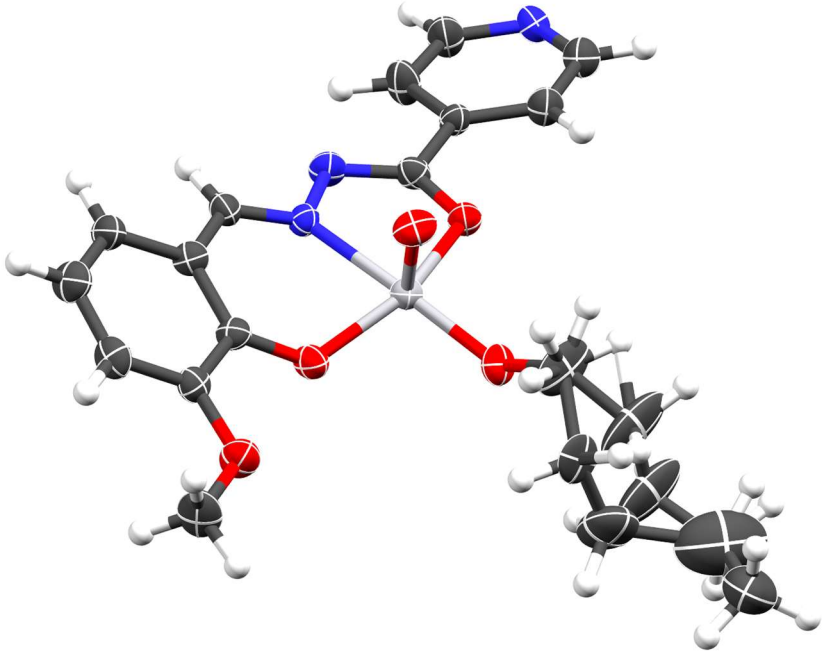

(e)

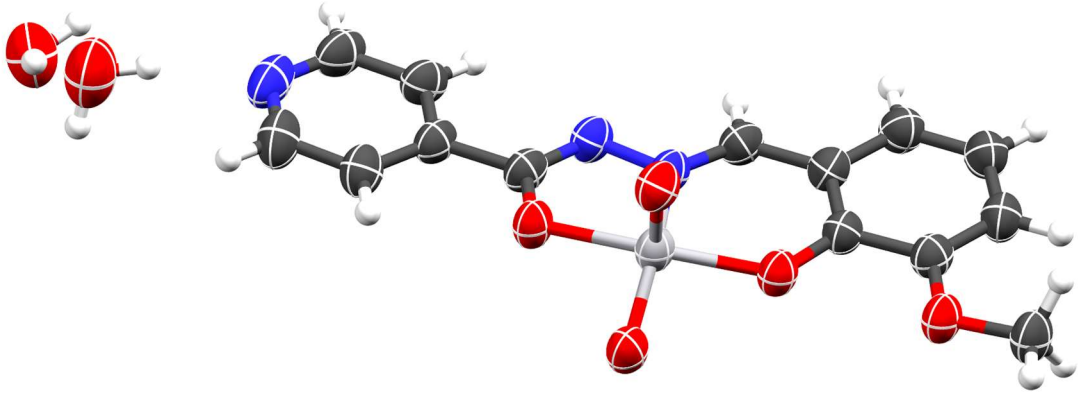

(f)

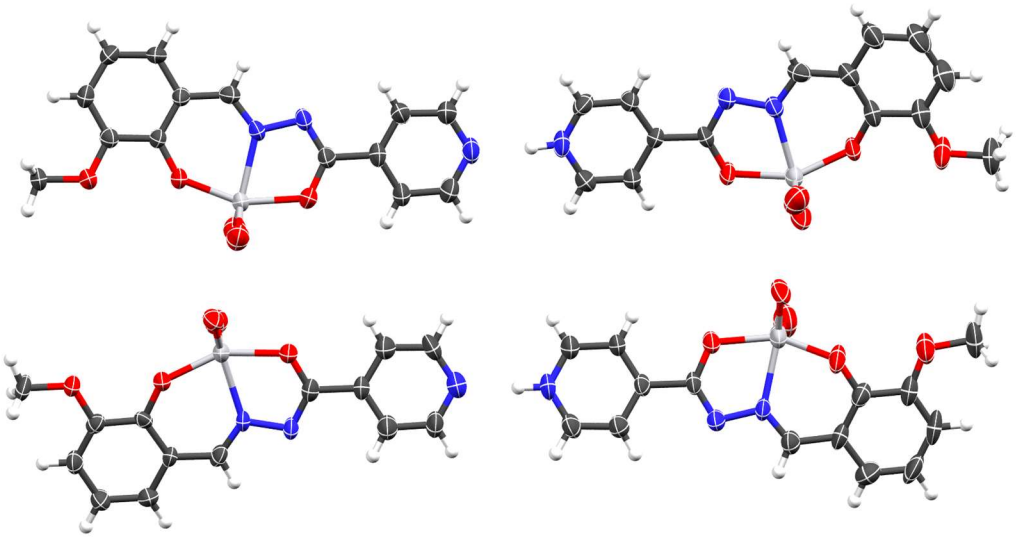

(g)

Fig. S2 Asymmetric units of (a) **1**, (b) **2**, (c) **3**, (d) **4**, (e) **5**, (f) **6·2H$_2$O** and (g) **6·0.5H$_2$O·0.5CH$_3$OH**. Atoms are shown as thermal ellipsoids with 50% probability level. Disorder of *n*-butoxy and *n*-pentoxy ancillary ligands in **4** and **5**, respectively, was modelled as two split chains with common initial and terminal atoms.

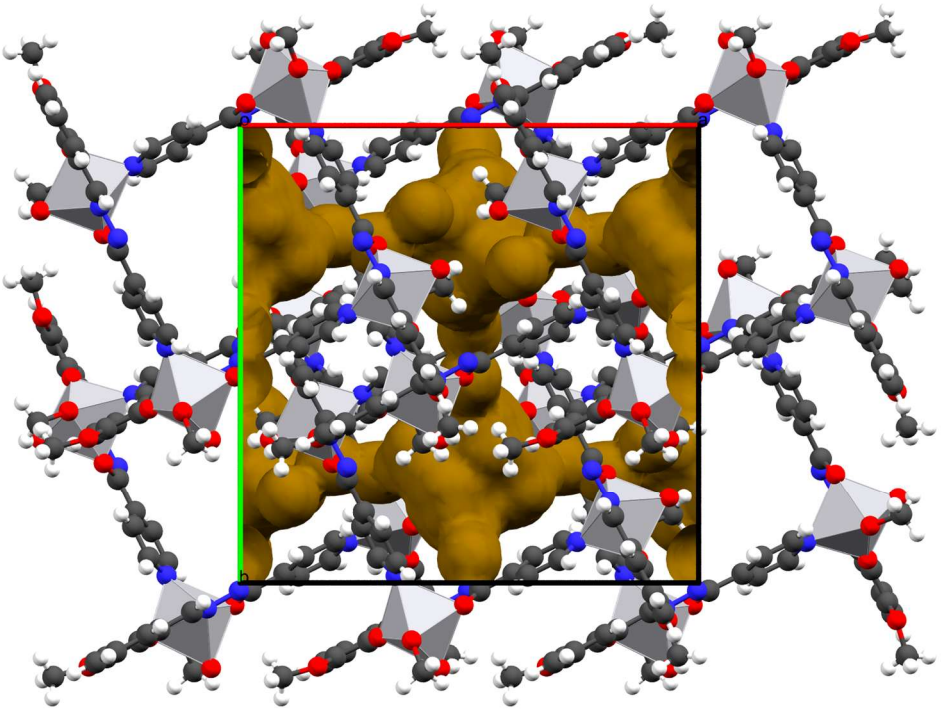

(a)

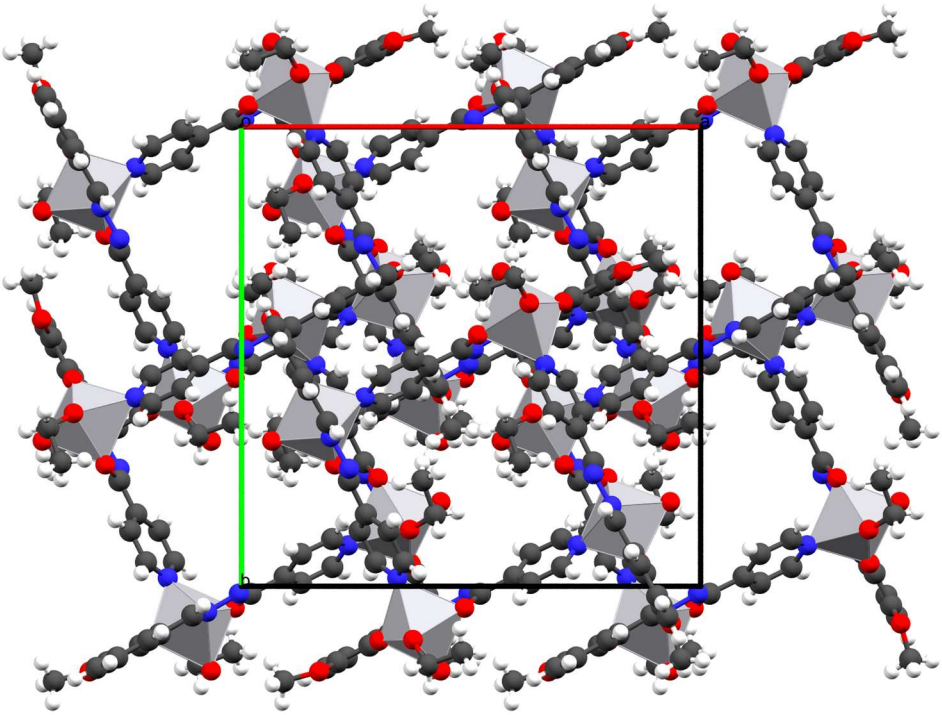

(b)

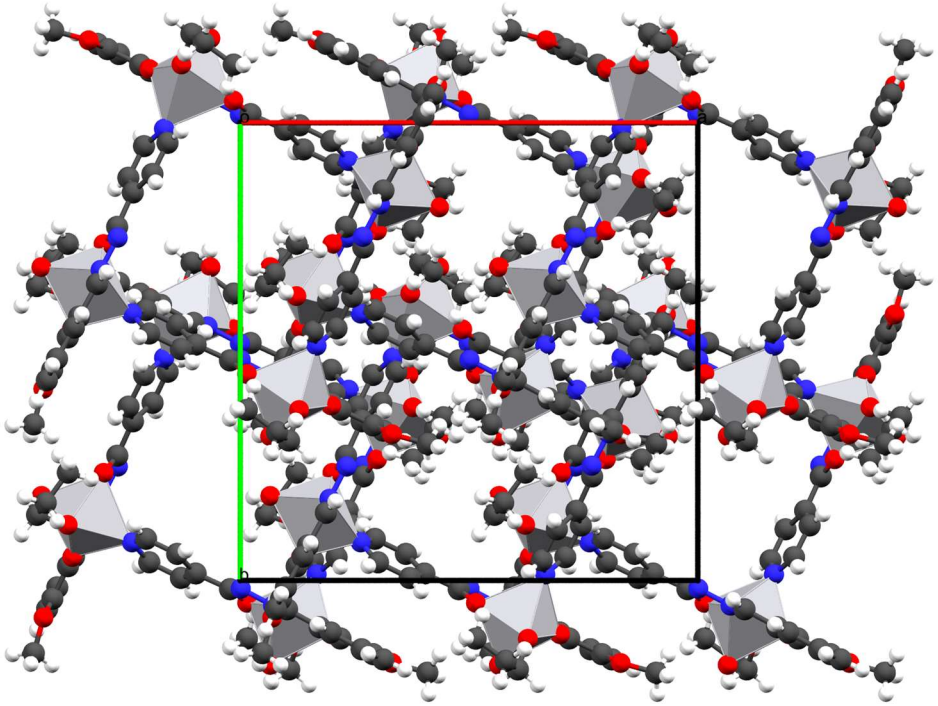

(c)

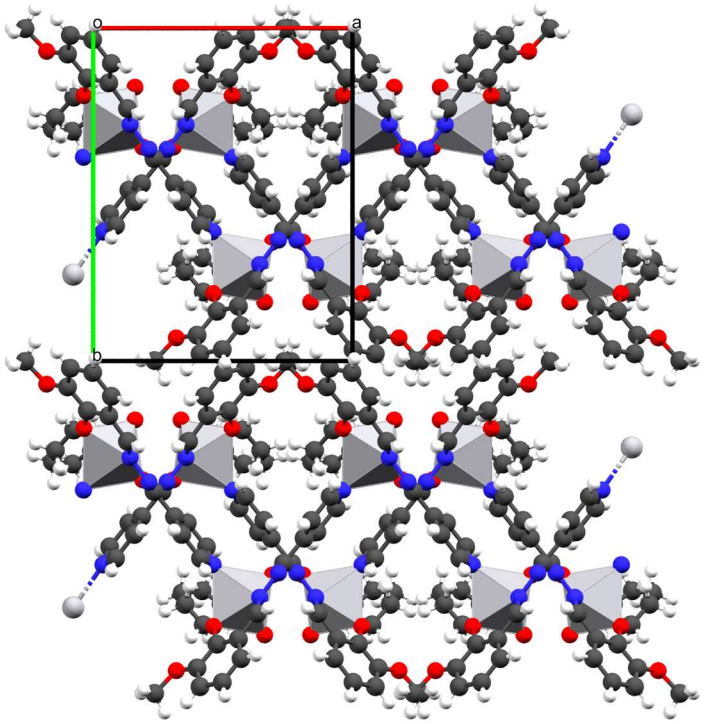

(d)

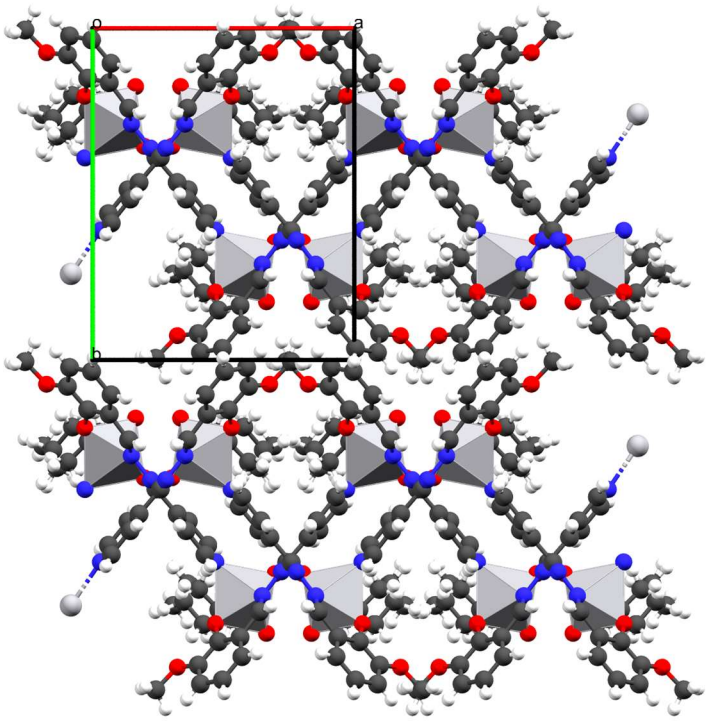

(e)

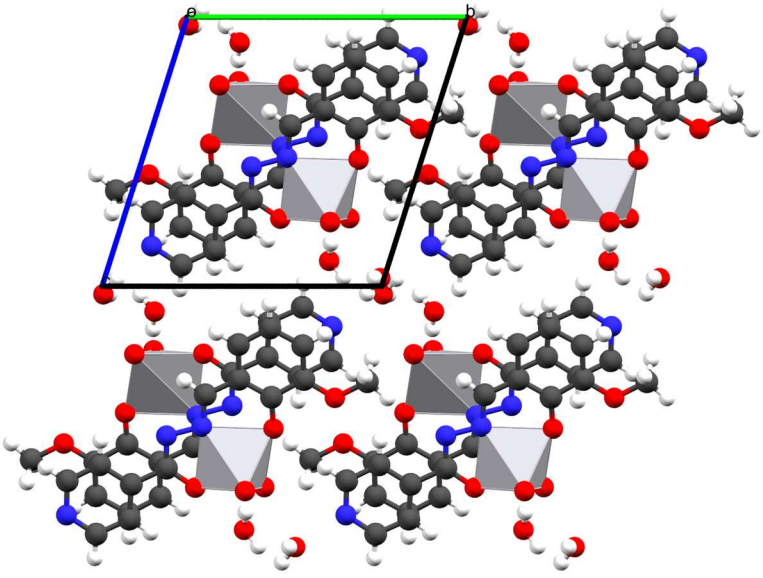

(f)

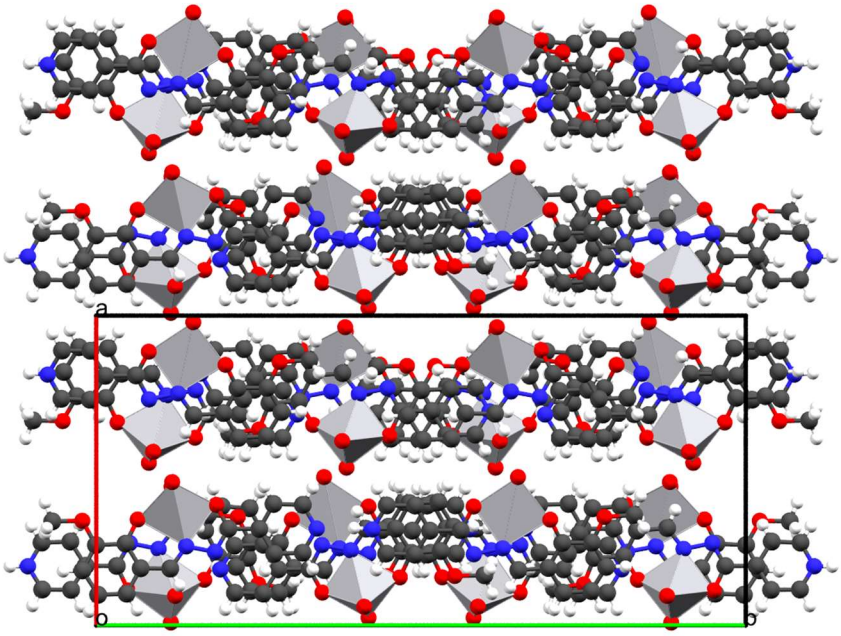

(g)

Fig. S3 Packing of molecules/polymeric chains in (a) **1**, (b) **2**, (c) **3**, (d) **4**, (e) **5**, (f) **6·2H$_2$O** and (g) **6·0.5H$_2$O·0.5CH$_3$OH**, shown in polyhedral style. **1**, **2** and **3** as one group, and **4** and **5** as the other group can be considered isostructural groups. Voids in **1** are represented by the yellow surface. Pseudopolymorphs of **6** pack as discrete irregularly shaped molecules.

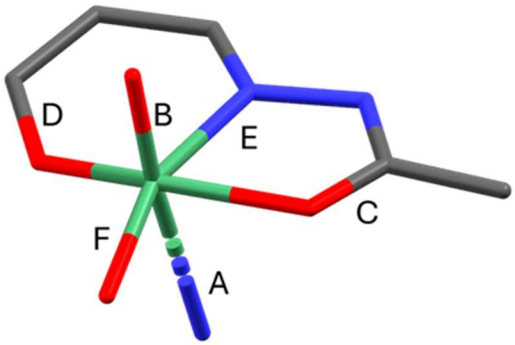

Compound	A	B	C	D	E	F
1	2.420(2)	1.586(2)	1.961(2)	1.844(2)	2.131(2)	1.779(2)
2	2.404(2)	1.592(2)	1.966(2)	1.850(2)	2.131(2)	1.776(2)
3	2.439(2)	1.587(2)	1.965(2)	1.848(2)	2.136(2)	1.772(2)
4	2.379(5)	1.595(4)	1.990(4)	1.866(4)	2.125(5)	1.775(4)
5	2.400(5)	1.594(4)	1.980(4)	1.865(5)	2.120(6)	1.773(6)
6·2H_2O	N/A	1.636(2)	1.994(2)	1.910(2)	2.128(2)	1.632(2)
6·0.5H_2O·0.5CH_3OH*	N/A	1.617	1.965	1.913	2.138	1.611

* average on 4 molecules in a.s.u.

Fig. S4 Bond lengths (Å) in the coordination sphere of the vanadium ion. Orange shading – tetranuclear complexes, blue shading – polymers, violet shading – mononuclear complexes.

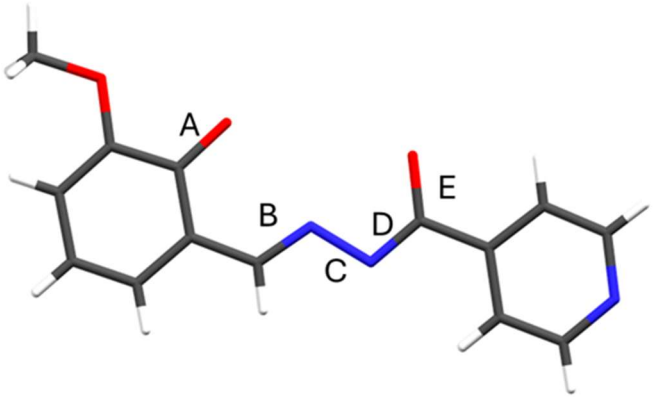

Compound	A	B	C	D	E
1	1.338(3)	1.287(3)	1.403(3)	1.303(3)	1.302(3)
2	1.334(4)	1.297(4)	1.404(4)	1.301(4)	1.298(4)
3	1.321(4)	1.278(4)	1.402(4)	1.300(4)	1.298(4)
4	1.337(8)	1.291(8)	1.398(8)	1.301(8)	1.302(8)
5	1.347(9)	1.280(9)	1.392(7)	1.299(8)	1.301(8)
6·2H$_2$O	1.316(4)	1.293(4)	1.399(4)	1.290(4)	1.303(4)
6·0.5H$_2$O·0.5CH$_3$OH*	1.329	1.279	1.405	1.298	1.287

* average on 4 molecules in a.s.u.

Fig. S5 Bond lengths (Å) of the ligand dianion VIH^{2-}. Orange shading – tetranuclear complexes, blue shading – polymers, violet shading – mononuclear complexes. The bond lengths conform to the enolato-imino tautomeric form.

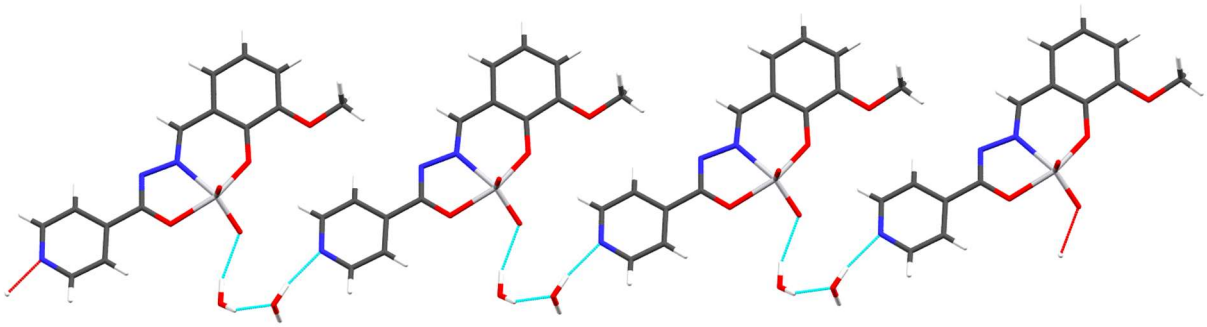

Fig. S6 Hydrogen-bonded chains of **6** in the crystal structure of **6·2H$_2$O.** Supramolecular chains are established through peculiar V=O···H–O(H) ···H–O(H) ···N$_{py}$ hydrogen bond composition.

Table S4. Experimental and crystallographic data for **8.**

Identifier	**8**
Empirical formula	$C_{16}H_{17}MoN_3O_6$
M_r	443.26
T/K	293(2)
Crystal system	triclinic, orange block
Space group	$P\,\bar{1}$
a/Å	7.28057(4)
b/Å	10.45368(5)
c/Å	12.64056(6)
α/°	113.2670(4)
β/°	96.4325(4)
γ/°	97.8303(4)
V/Å^3	860.915(8)
Z	2
ρ_{calc}/g cm^{-3}	1.710
μ/mm^{-1}	6.596
F(000)	448
Crystal size/mm^3	0.264×0.213×0.146
Radiation	Cu Kα (λ = 1.54184Å)
2Θ range/°	7.742 to 159.776
Index ranges	$-7 \le h \le 9$, $-13 \le k \le 13$, $-16 \le l \le 16$
Reflections collected	32258
Independent reflections	3704 [R_{int} = 1.56%, R_{sigma} = 3.57 %]
Data/restraints/parameters	3704/-/242
g_1, g_2 in w[a]	0.0255, 0.4301
Goodness–of–fit on F^2, S[b]	1.076
Final R and wR[c] values [$I \ge 2\sigma(I)$]	R_1 = 1.97%, wR_2 = 5.15%
Final R and wR[c] values [all data]	R_1 = 1.99%, wR_2 = 5.16%
Largest diff. peak/hole / e Å^{-3}	0.368/–0.411

[a] $w = 1/[\sigma F_o^2 + (g_1P)^2 + g_2P]$ where $P = (F_o^2 + 2F_c^2)/3$
[b] $S = \{\Sigma[w(F_o^2 - F_c^2)2]/(N_r - N_p)\}^{1/2}$ where N_r = number of independent reflections, N_p = number of refined parameters.
[c] $R = \Sigma||F_o| - |F_c||/\Sigma|F_o|$; $wR = \{\Sigma[w(F_o^2 - F_c^2)2]/\Sigma[w(F_o^2)2]\}^{1/2}$

Compound [MoO_2(VIH)(C_2H_5OH)] (**8**) crystallizes in triclinic space group $P\bar{1}$ with one molecule of complex in the a.s.u. The dioxomolybdenum(VI) metal core is coordinated by the *ONO* chelating pocket of the doubly deprotonated VIH ligand in enolato-imino form. Sixth coordination place is occupied by ethanol molecule, which forms hydrogen bond with the pyridyl nitrogen atom of the neighbouring molecule, forming a supramolecular dimer.

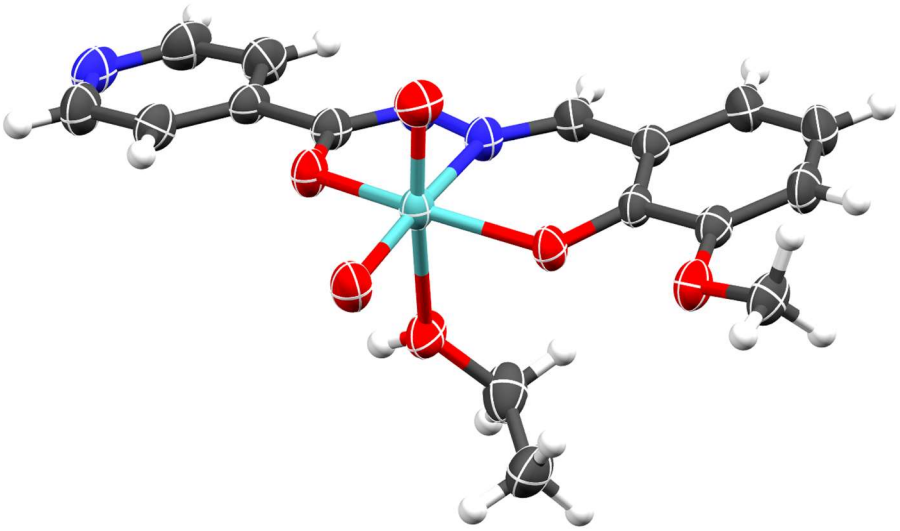

(a)

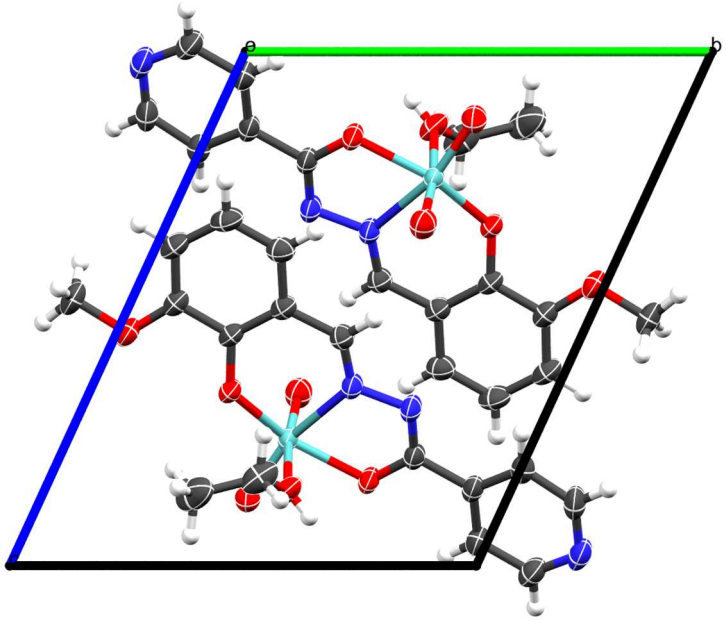

(b)

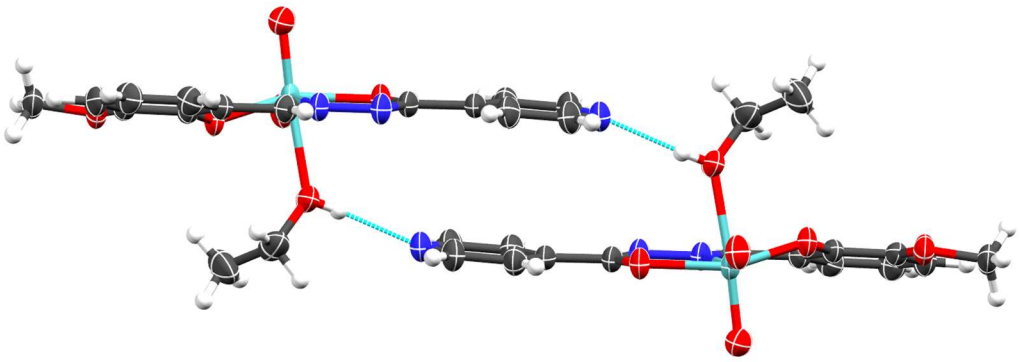

(c)

Fig. S6 a) Asymmetric unit of **8** with atoms shown as thermal ellipsoids with 50% probability level. b) Packing of molecules in **8** shown along *a* crystallographic axis. c) Hydrogen-bonded supramolecular dimers of **8**. Hydrogen bond is formed between pyridyl nitrogen atom and ethanol hydroxy group.

1.3. UV-Vis spectroscopy

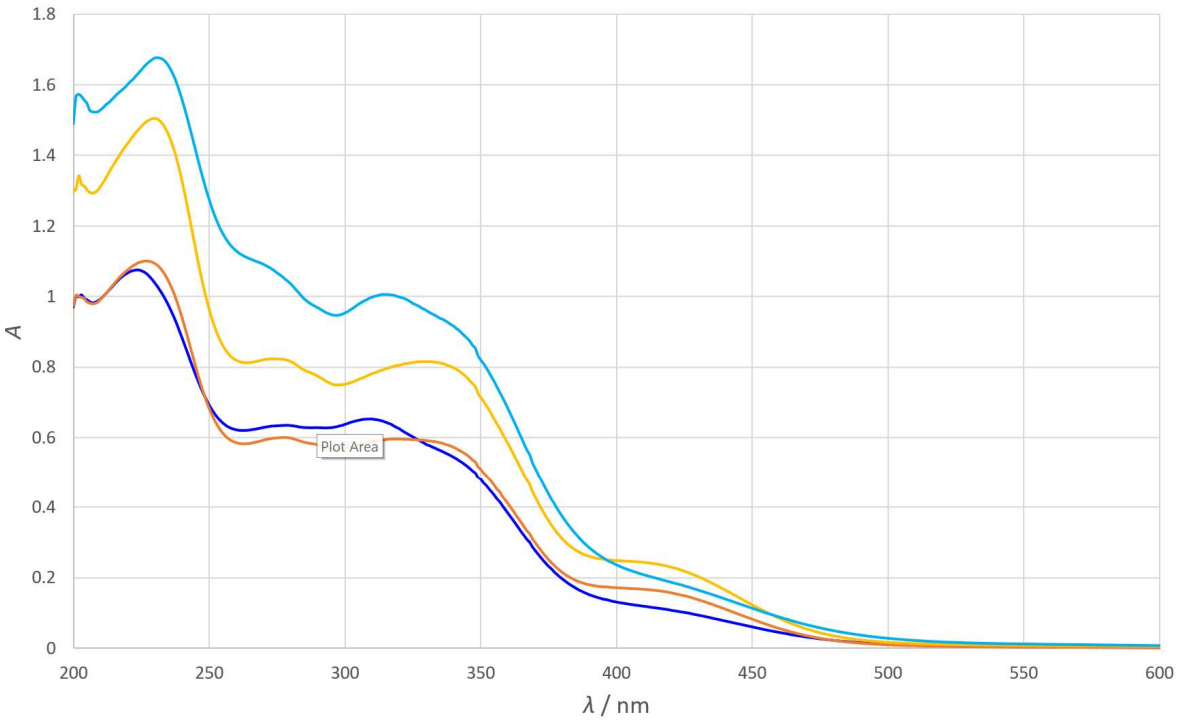

Fig. S7 UV-Vis spectra of: reaction mixture of NH_4VO_3 (c_0 = 4.0×10^{-5} mol dm^{-3}) and H_2VIH (c_0 = 4.0×10^{-5} mol dm^{-3}) in methanol after 10 min (blue) and 16.5 h (orange); complex $[VO_2(VIH)]$ (**6**) (c = 6.0×10^{-5} mol dm^{-3}) in methanol (yellow); complex $[VO(VIH)(OCH_3)]_4$ (**1**) (c = 1.5×10^{-5} mol dm^{-3}) in methanol (light blue).

Table S5 UV-Vis spectral data of H_2VIH and its complexes in both methanol and acetonitrile

Compound	Solvent	λ_{max}/nm (ε/dm^3 mol^{-1} cm^{-1})
H_2VIH	CH_3OH	221 (2.21·10^4), 304 (1.83·10^4), 342[a]
	CH_3CN	229 (1.58·10^4), 300 (2.06·10^4), 342[a]
$[VO(VIH)(OCH_3)]_4$	CH_3OH	231 (1.10·10^5), ~272[a], 315 (6.62·10^4), ~340[a], ~425[a]
	CH_3CN	232 (7.56·10^4), 275 (5.16·10^4), 339 (4.27·10^4), 410[a]
$[VO(VIH)(OC_2H_5)]_4$	CH_3OH	231 (1.04·10^5), ~272[a], 315 (6.23·10^4), ~340[a], ~425[a]
	CH_3CN	234 (7.82·10^4), 270 (6.09·10^4), 320[a], 410[a]
$[VO(VIH)(OC_3H_7)]_4$	CH_3OH	231 (1.19·10^5), ~272[a], 315 (7.15·10^4), ~340[a], ~425[a]
	CH_3CN	234 (7.05·10^4), 279 (4.93·10^4), 340 (4.13·10^4), 410[a]
$[VO(VIH)(OC_4H_9)]_n$	CH_3OH	231 (3.15·10^4), ~272[a], 315 (2.59·10^4), ~340[a], ~425[a]
	CH_3CN	234 (2.28·10^4), 279 (1.68·10^4), 340 (1.34·10^4), 410[a]
$[VO(VIH)(OC_5H_{11})]_n$	CH_3OH	231 (3.18·10^4), ~272[a], 315 (1.92·10^4), ~340[a], ~425[a]
	CH_3CN	234 (2.14·10^4), 279 (1.54·10^4), 340 (1.24·10^4), 410[a]
$[VO_2(HVIH)]$	CH_3OH	230 (2.51·10^4), 276 (1.37·10^4), 330[b] (1.36·10^4), 410 (4.05·10^3)
	CH_3CN	234 (2.48·10^4), 275 (1.42·10^4), 339 (1.41·10^4), 410 (6.80·10^3)
$[MoO_2(VIH)]_4$	CH_3OH	225 (1.04·10^5), 280 (4.95·10^4), 317 (4.37·10^4), ~365[a], ~420[a]
	CH_3CN	231 (9.25·10^4), 275 (5.23·10^4), ~315[a], 360[a], ~425[a]
$[MoO_2(VIH)(C_2H_5OH)]$	CH_3OH	225 (2.58·10^4), 280 (1.23·10^4), 317 (1.08·10^4), ~365[a], ~420[a]
	CH_3CN	231 (2.54·10^4), 275 (1.43·10^4), ~315[a], 360[a], ~425[a]

[a] Shoulder.

[b] Broad.

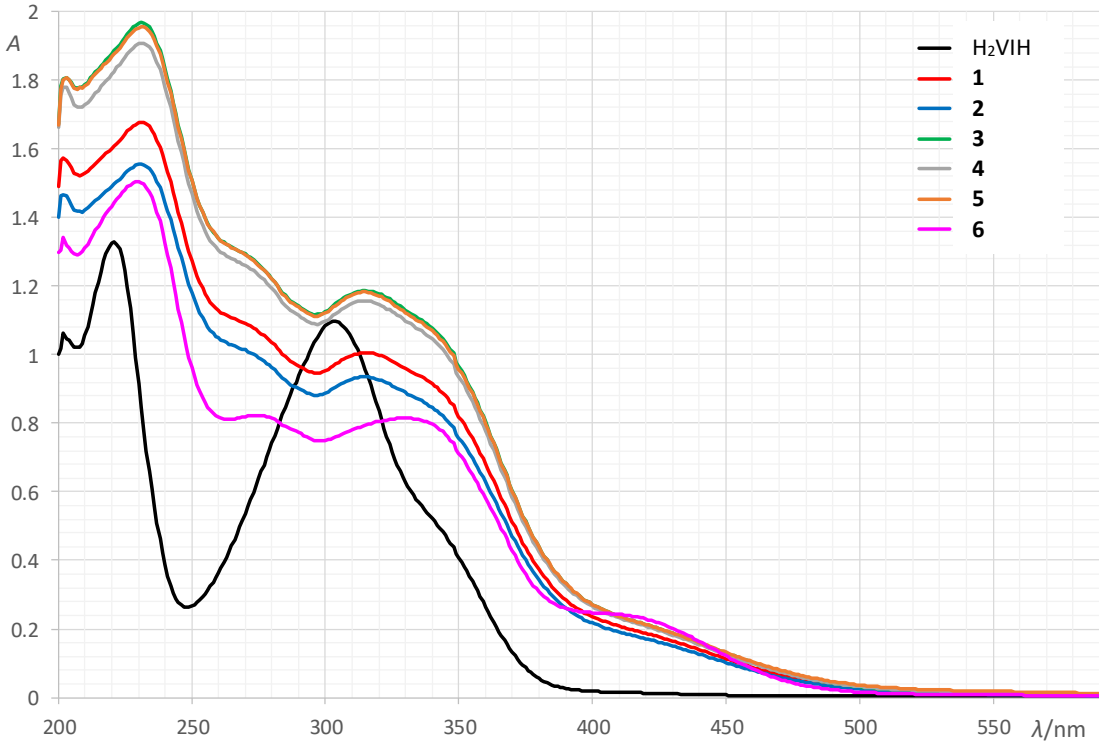

Fig. S8 The UV-Vis spectra of H_2VIH and its vanadium(V) complexes **1**–**6** in methanol. The concentration is 6.0×10^{-5} mol dm^{-3} for H_2VIH and **6**. The concentration of complexes **1**–**5** is 1.5×10^{-5} mol dm^{-3}.

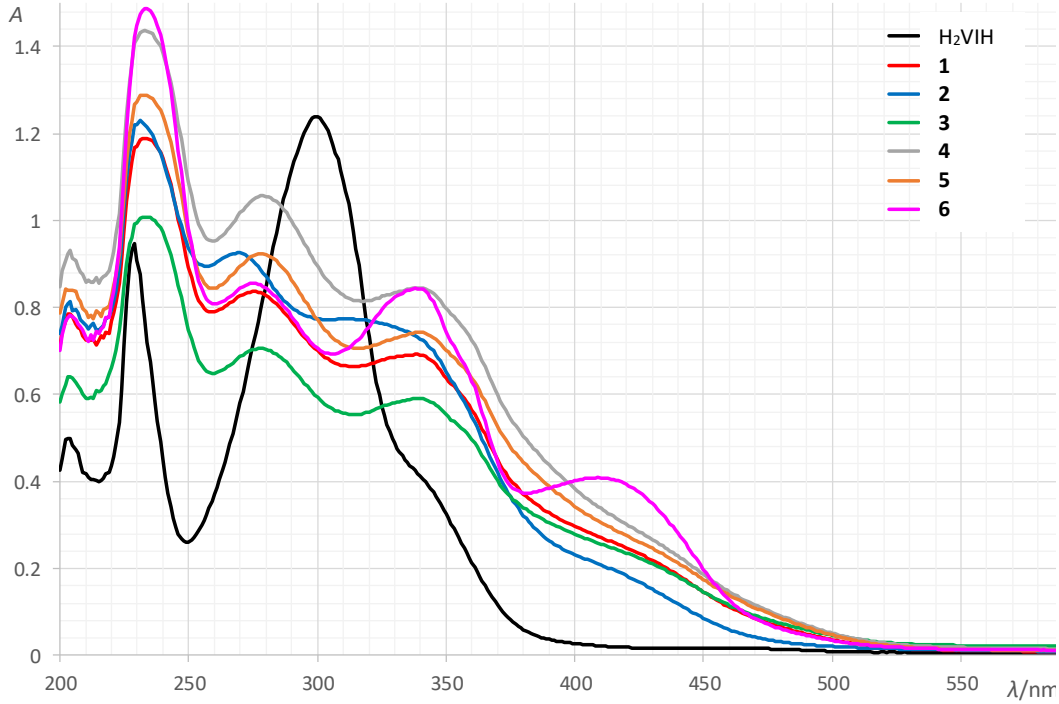

Fig. S9 The UV-Vis spectra of H_2VIH and its vanadium(V) complexes **1**–**6** in acetonitrile. The concentration is 6.0×10^{-5} mol dm^{-3} for H_2VIH and **6**. The concentration of complexes **1**–**5** is 1.5×10^{-5} mol dm^{-3}.

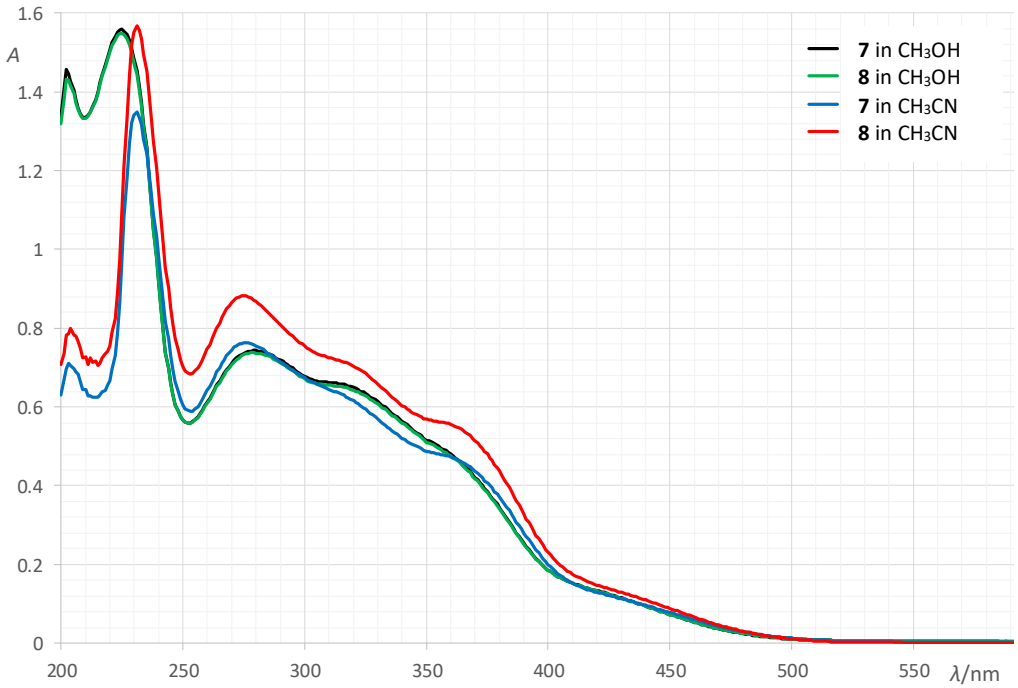

Fig. S10 The UV-Vis spectra of molybdenum(VI) complexes **7** and **8** in both methanol and acetonitrile. The concentration is 1.5×10^{-5} mol dm^{-3} for **7** and 6.0×10^{-5} mol dm^{-3} for **8**.

1.4. NMR spectroscopy

Table S6 ^{1}H and ^{13}C chemical shifts (ppm) of H_2VIH, $[VO(VIH)(OCH_3)]_4$, and $[MoO_2(VIH)]_4$

Atom	**H_2VIH**		**$[VO(VIH)(OCH_3)]$**		**$[MoO_2(VIH)]_4$**	
	δ / ppm (^{1}H)	δ / ppm (^{13}C)	δ / ppm (^{1}H)	δ / ppm (^{13}C)	δ / ppm (^{1}H)	δ / ppm (^{13}C)
1	8.65	150.11	8.83	154.39	8.92	158.63
4	–	162.59	–	169.37	–	167.69
5	–	140.97	–	139.97	–	138.92
6	7.92	121.77	8.07	122.41	8.05	122.18
7	8.78	149.74	8.68	149.27	8.72	149.47
8	–	–			–	–
9	8.78	149.74	8.68	149.26	8.72	149.47
10	7.92	121.77	8.07	122.41	8.05	122.18
11	–	118.60	–	120.58	–	120.57
12	–	147.63	–	154.47	–	150.65
13	–	148.12	–	147.51	-	149.04
14	7.07	113.84	7.22	116.80	7.29	117.66
15	6.91	119.08	6.98	120.04	7.09	121.75
16	7.26	120.90	7.25	124.20	7.30	125.17
OCH_3	3.91	55.25	3.92	55.59	3.92	55.59

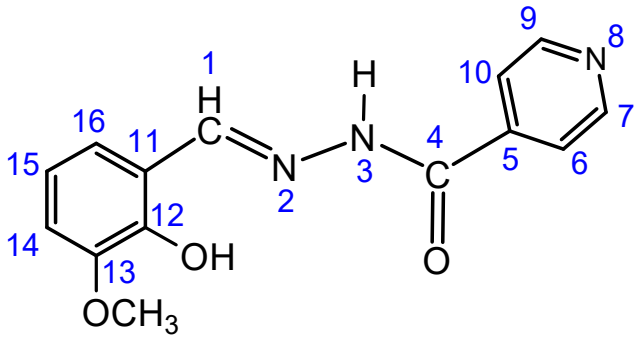

Scheme S1 The structural formula of H_2VIH with the NMR numbering scheme.

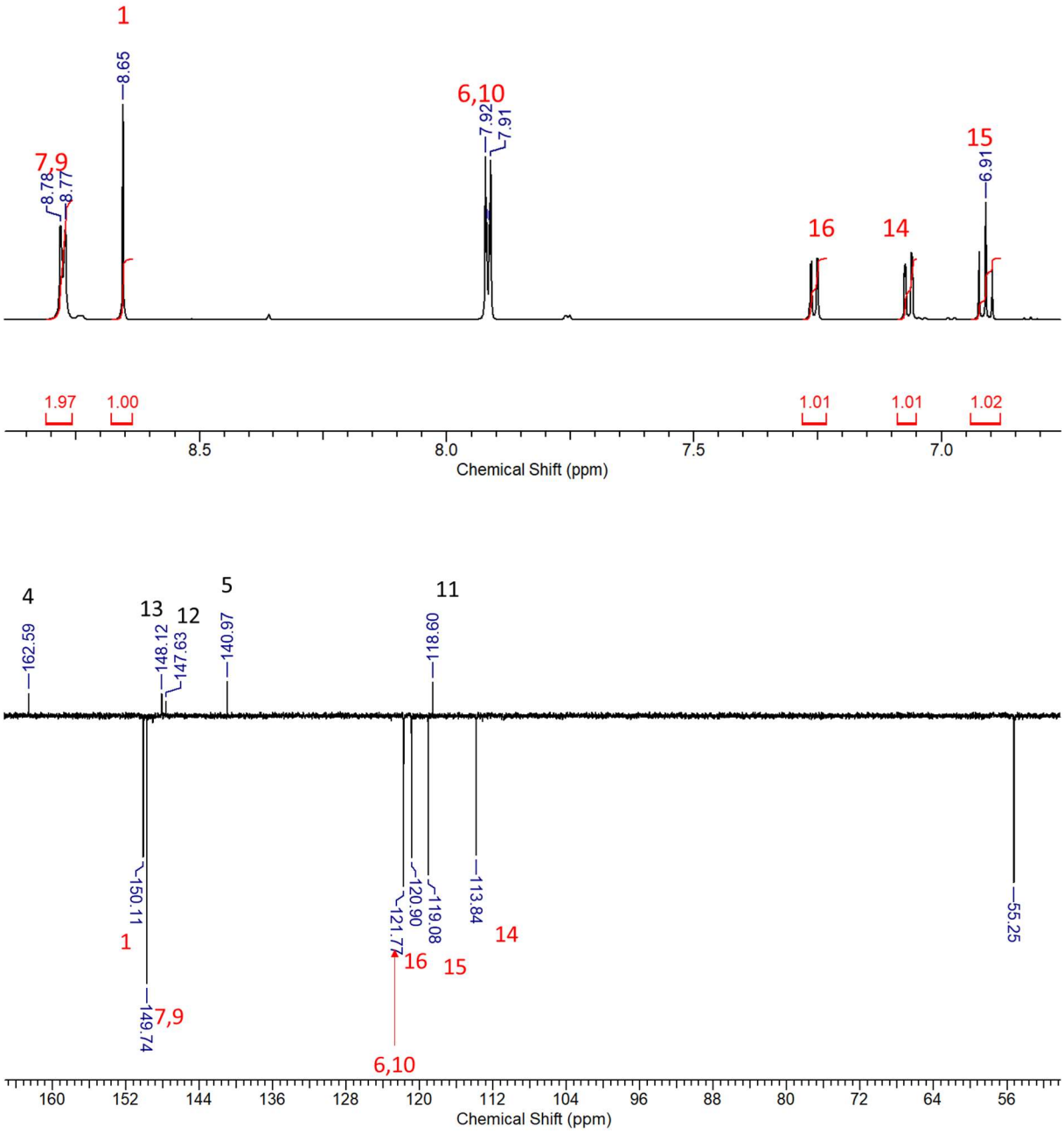

Fig. S11 A portion of the ^{1}H and ^{13}C NMR spectra of H_2VIH in CD_3OD.

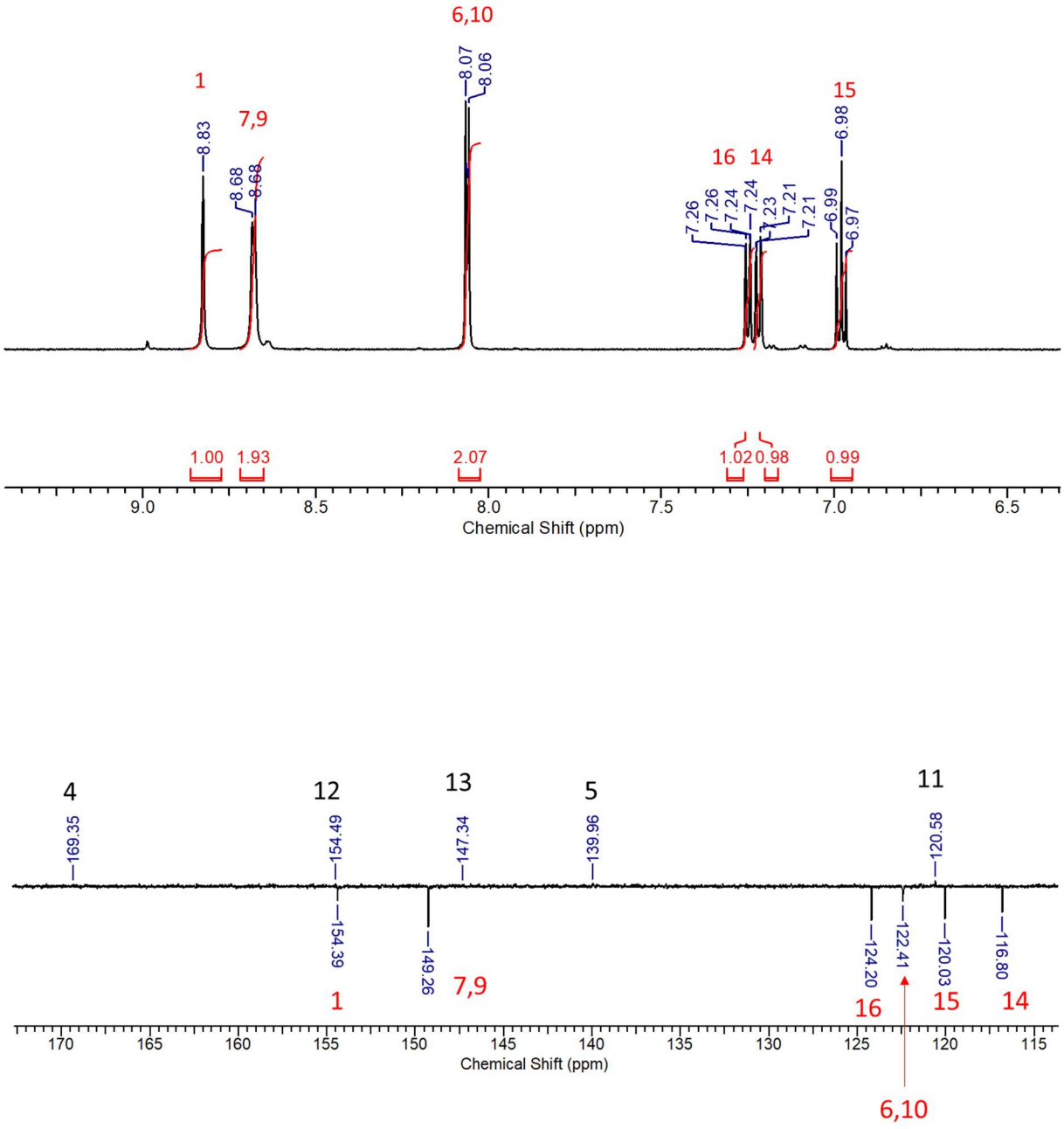

Fig. S12 A portion of the ^{1}H and ^{13}C NMR spectra of $[VO(VIH)(OCH_3)]_4$ in CD_3OD.

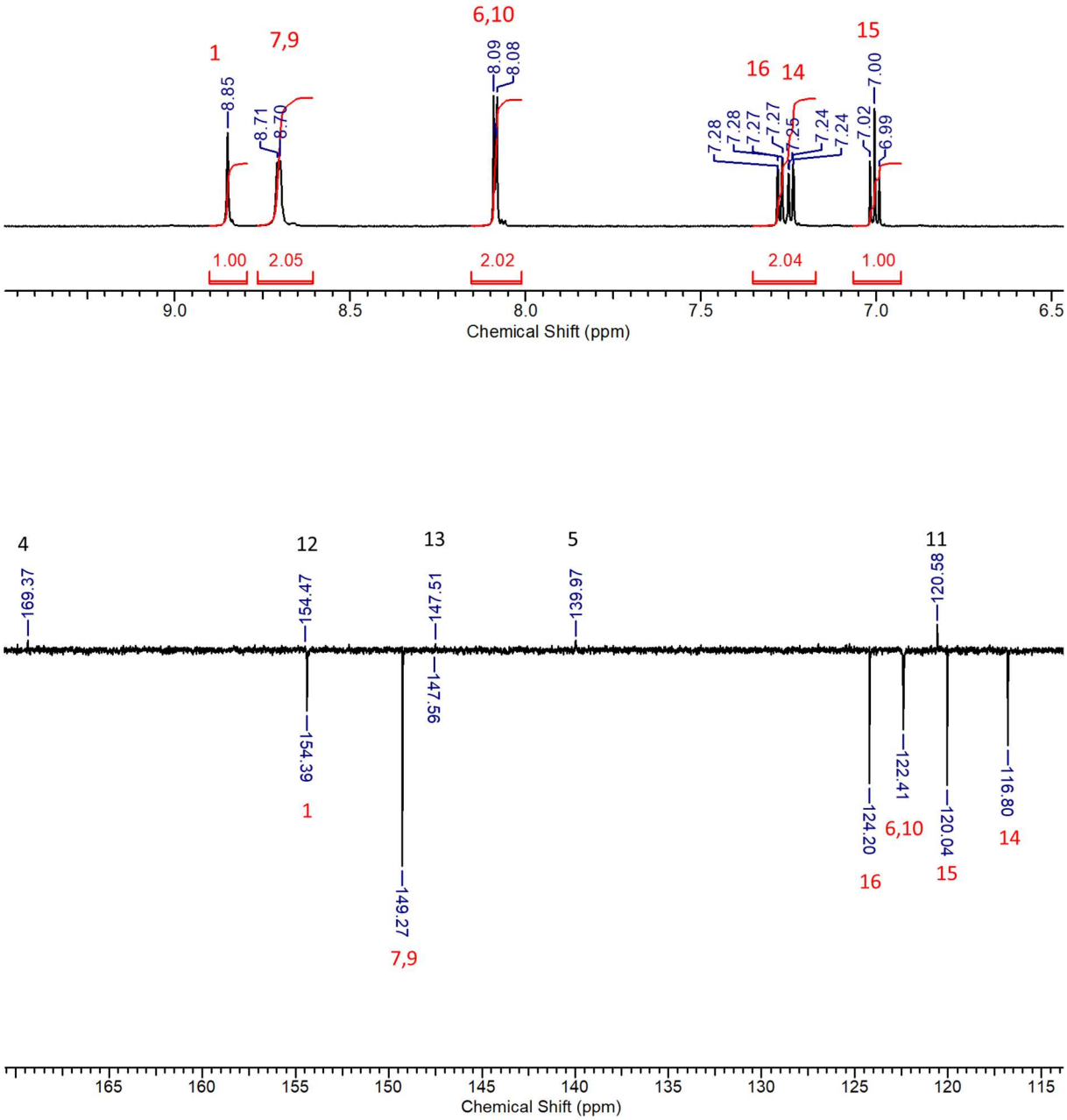

Fig. S13 A portion of the ^{1}H and ^{13}C NMR spectra of $[VO(VIH)(OC_4H_9)]_n$ in CD_3OD.

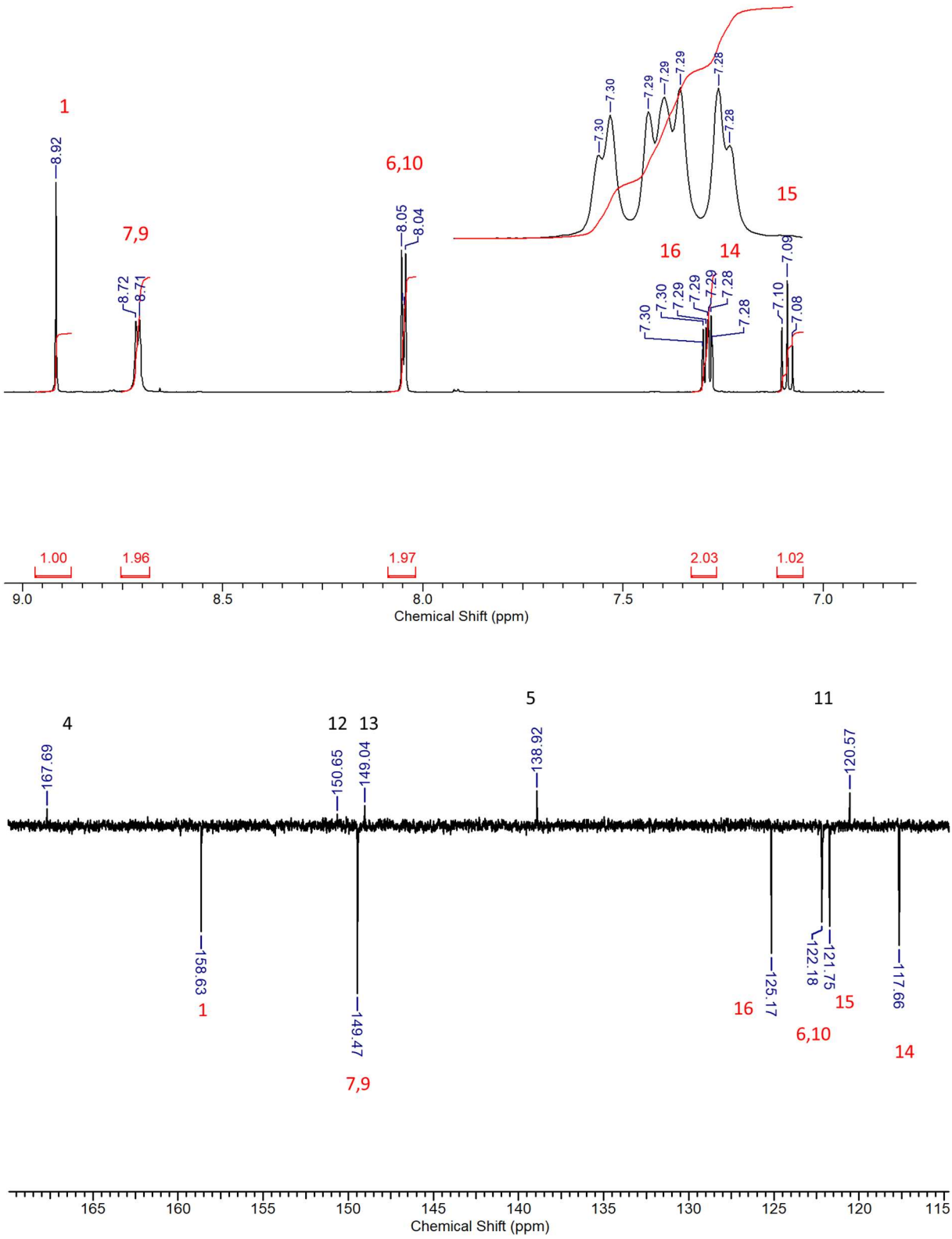

Fig. S14 A portion of the ^{1}H and ^{13}C NMR spectra of $[MoO_2(VIH)]_4$ in CD_3OD.

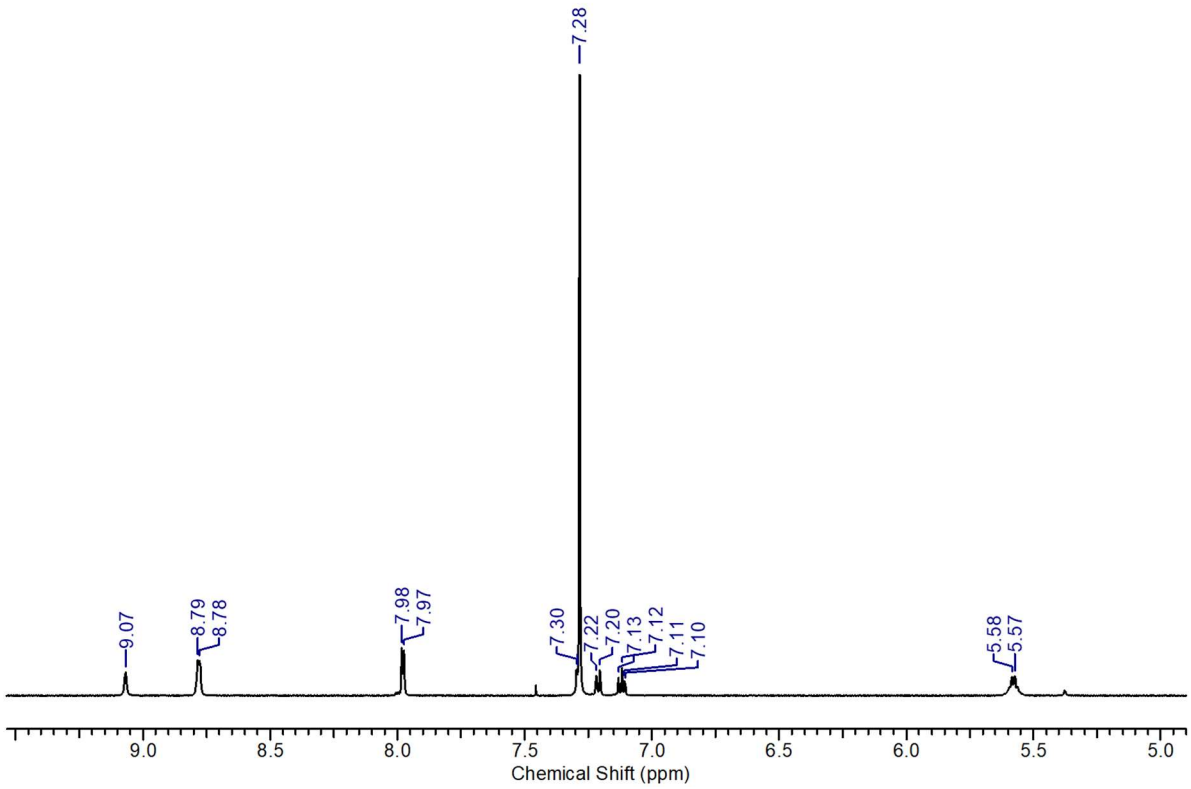

Fig. S15 A portion of the ^{1}H NMR spectrum of $[VO(VIH)(OC_3H_7)]_n$ in $CDCl_3$.

1.5. ATR-IR spectroscopy

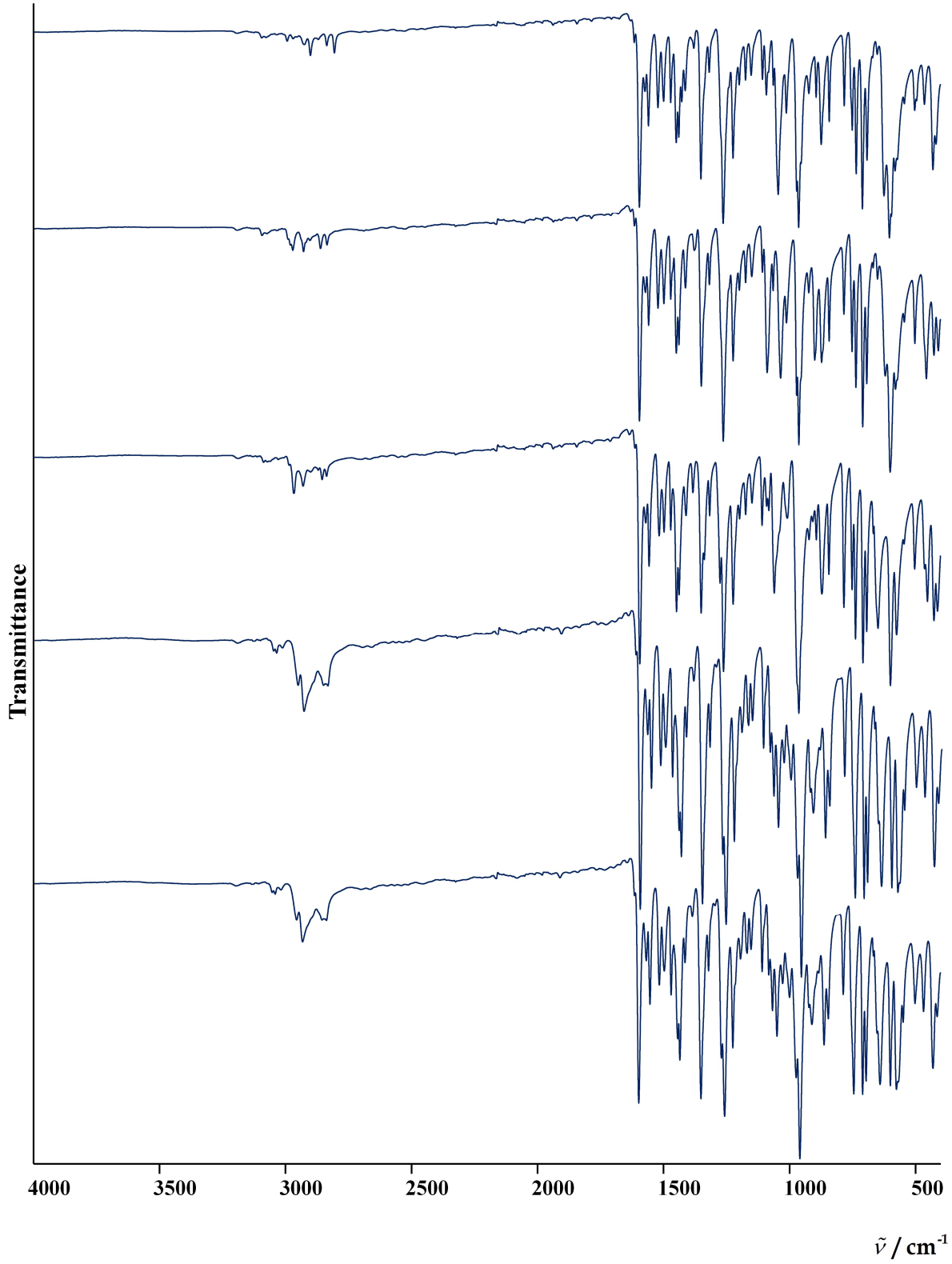

Fig. S16 Comparison of IR-ATR spectra of **1**, **2**, **3**, **4**, and **5** (from top to bottom).

1.6. TGA, TGA-FTIR

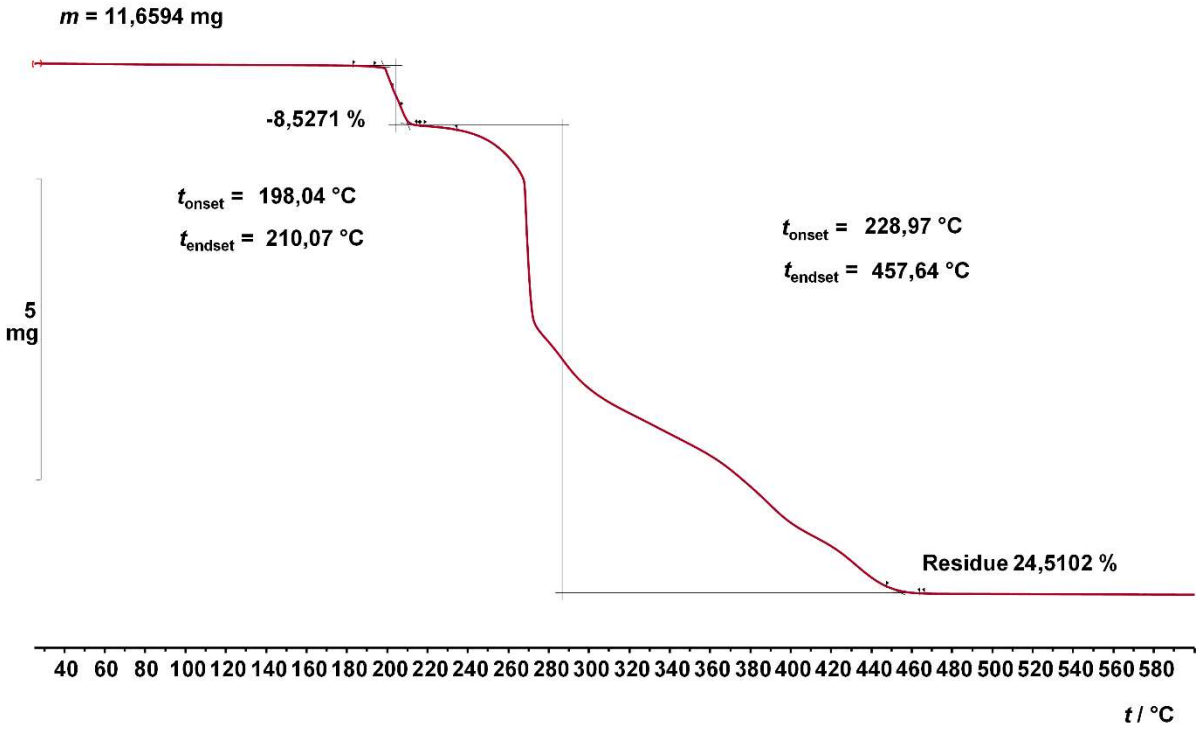

(a)

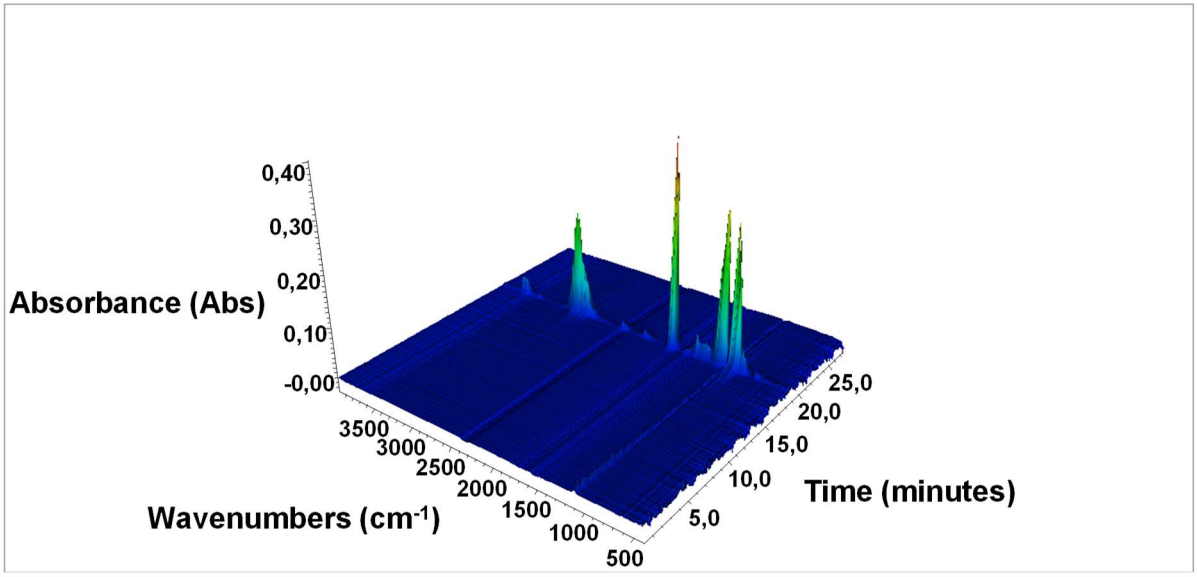

(b)

Fig. S17 (a) TGA curve of **1** under the O_2 atmosphere in the range of 25-600 °C (with a heating rate of 5 °C min^{-1}), (b) 3D FT-IR profile of the gas product evolved from **1** under the O_2 atmosphere in the range of 25-300 °C (with a heating rate of 10 °C min^{-1}).

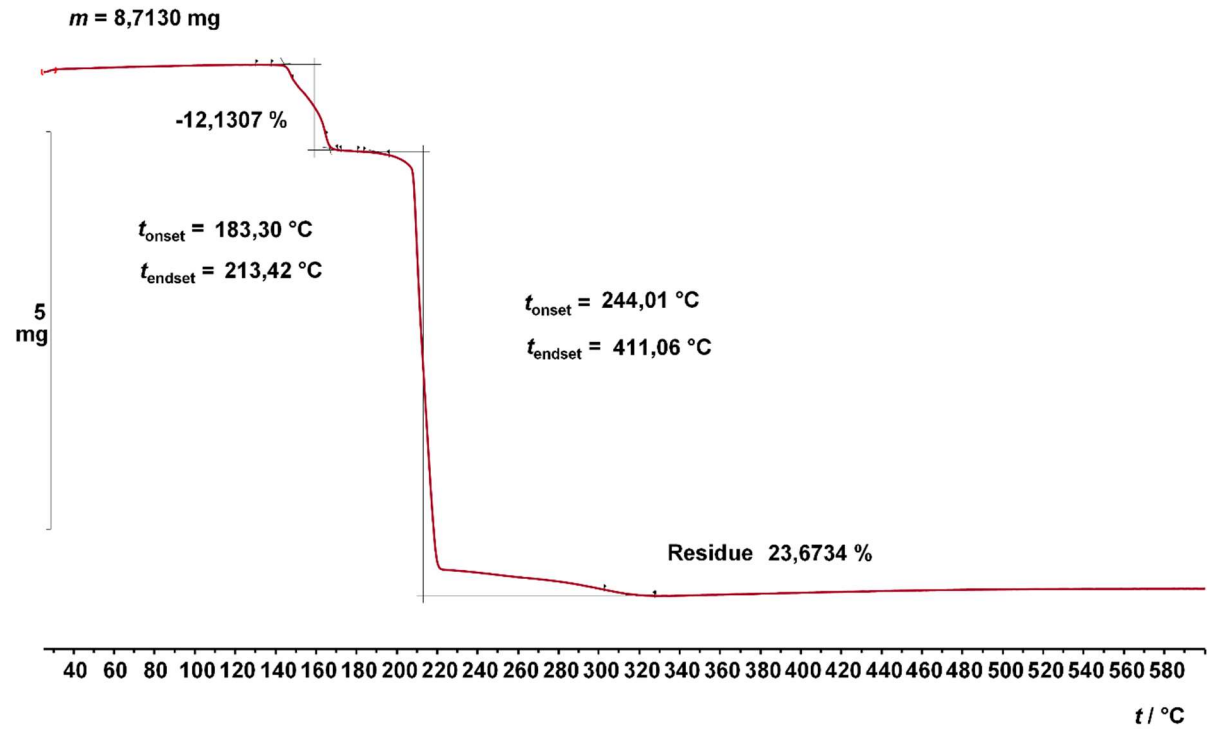

(a)

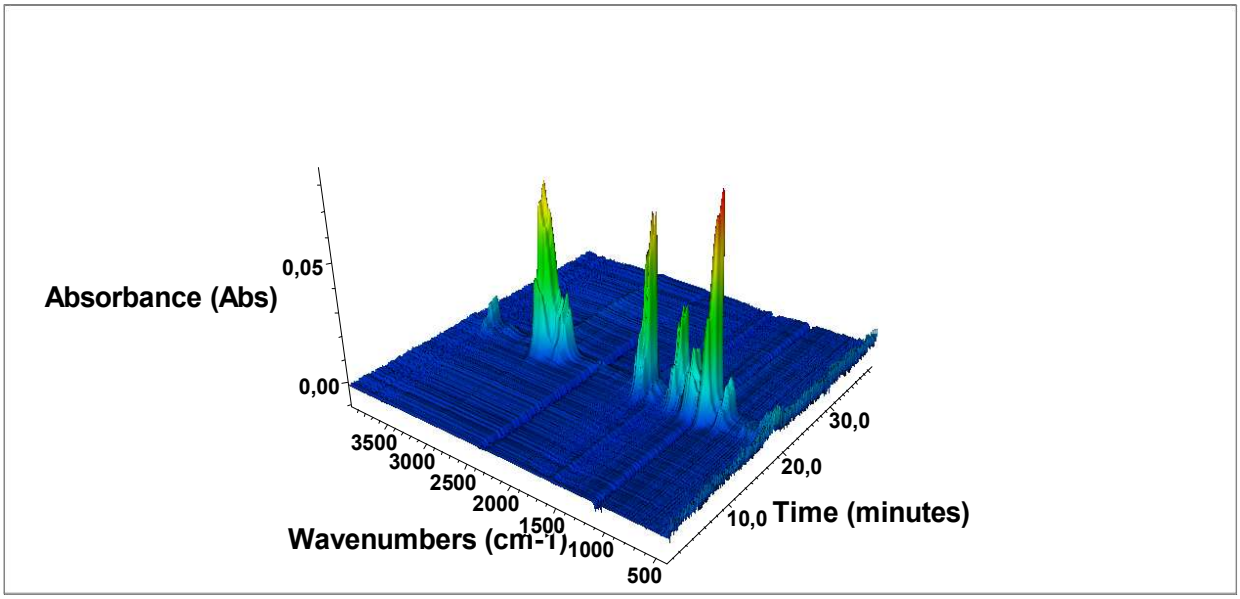

(b)

Fig. S18 (a) TGA curve of **2** under the O_2 atmosphere in the range of 25-600 °C (with a heating rate of 5 °C min^{-1}), (b) 3D FT-IR profile of the gas product evolved from **2** under the O_2 atmosphere in the range of 25-300 °C (with a heating rate of 10 °C min^{-1}).

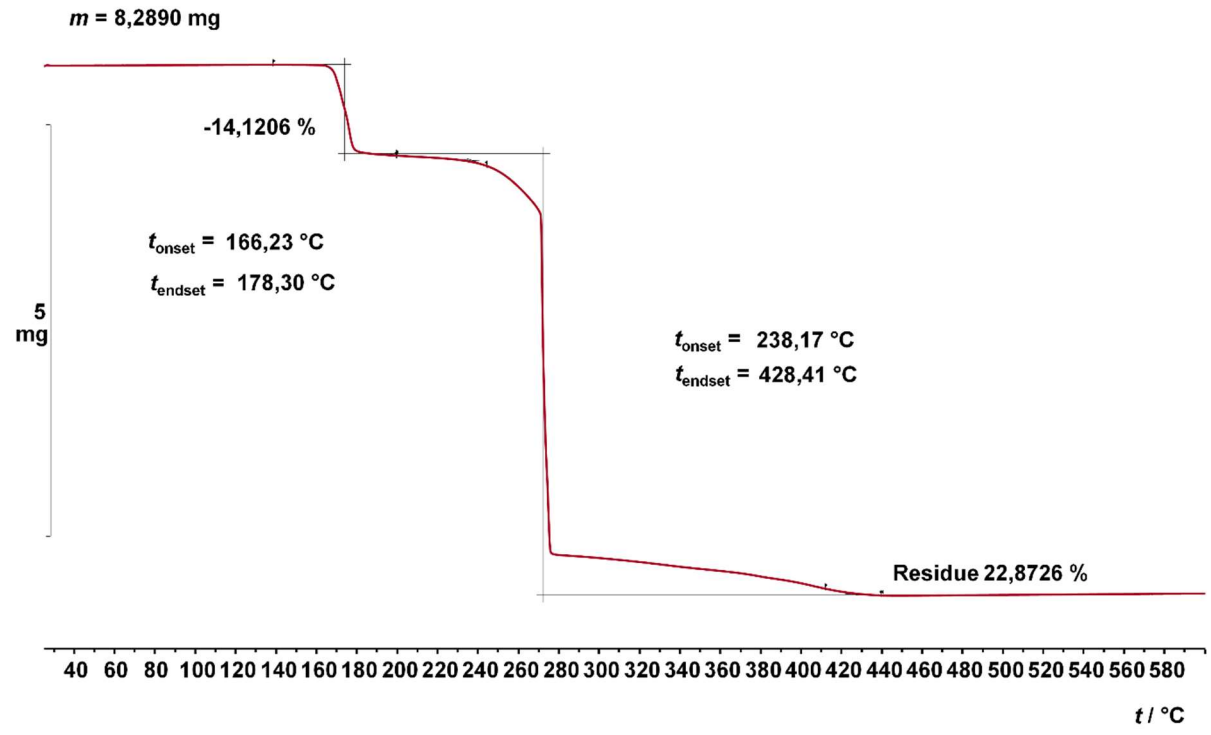

(a)

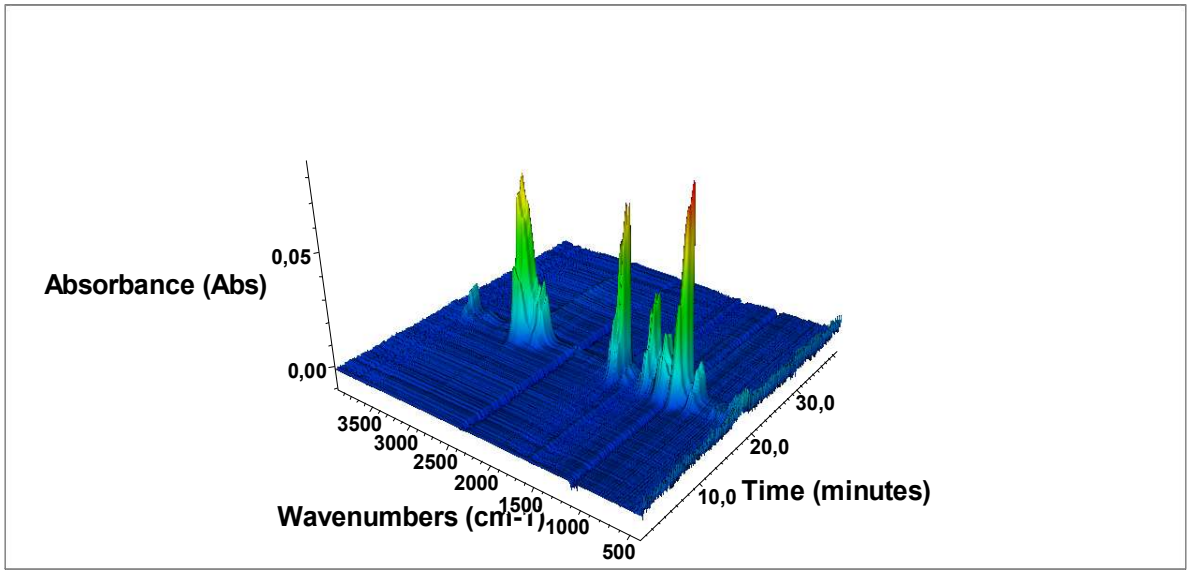

(b)

Fig. S19 (a) TGA curve of **3** under the O_2 atmosphere in the range of 25-600 °C (with a heating rate of 5 °C min^{-1}), (b) 3D FT-IR profile of the gas product evolved from **3** under the O_2 atmosphere in the range of 25-300 °C (with a heating rate of 10 °C min^{-1}).

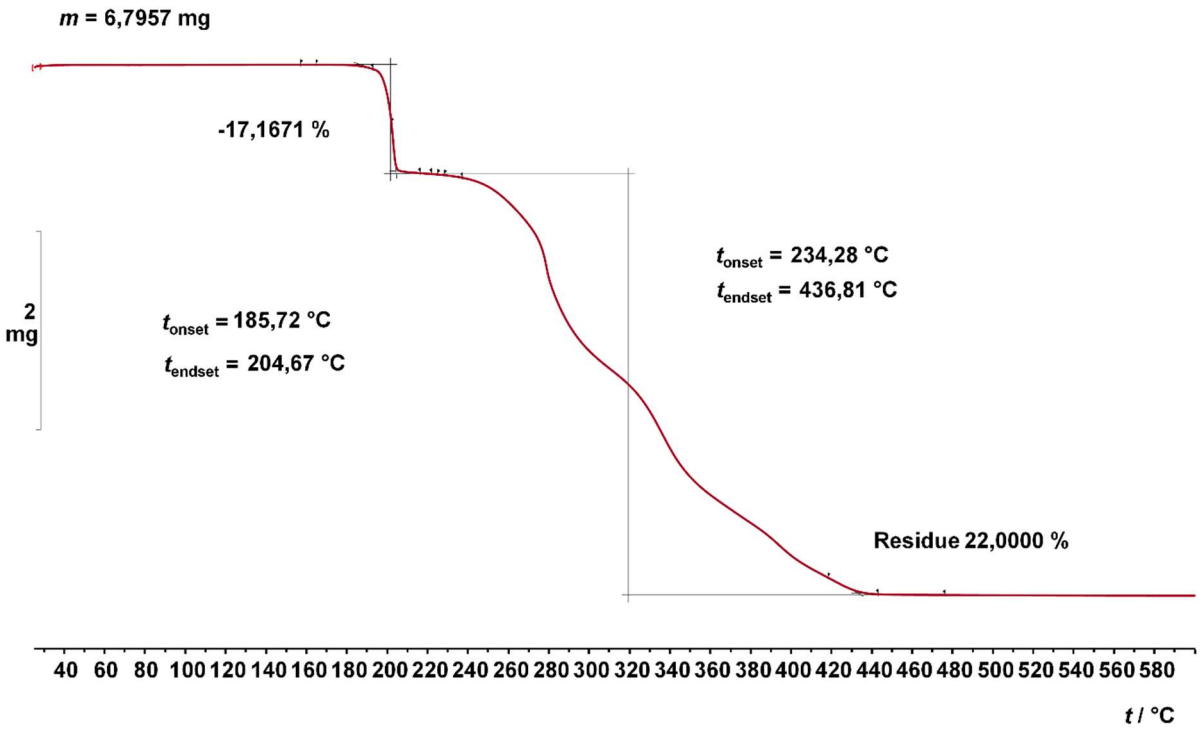

(a)

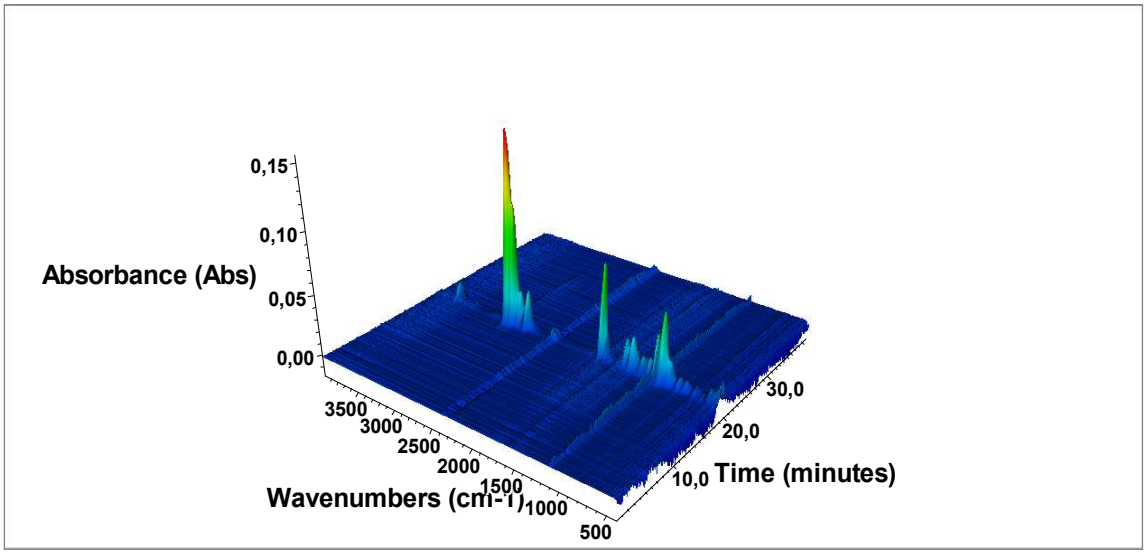

(b)

Fig. S20 (a) TGA curve of **4** under the O_2 atmosphere in the range of 25-600 °C (with a heating rate of 5 °C min^{-1}), (b) 3D FT-IR profile of the gas product evolved from **4** under the O_2 atmosphere in the range of 25-300 °C (with a heating rate of 10 °C min^{-1}).

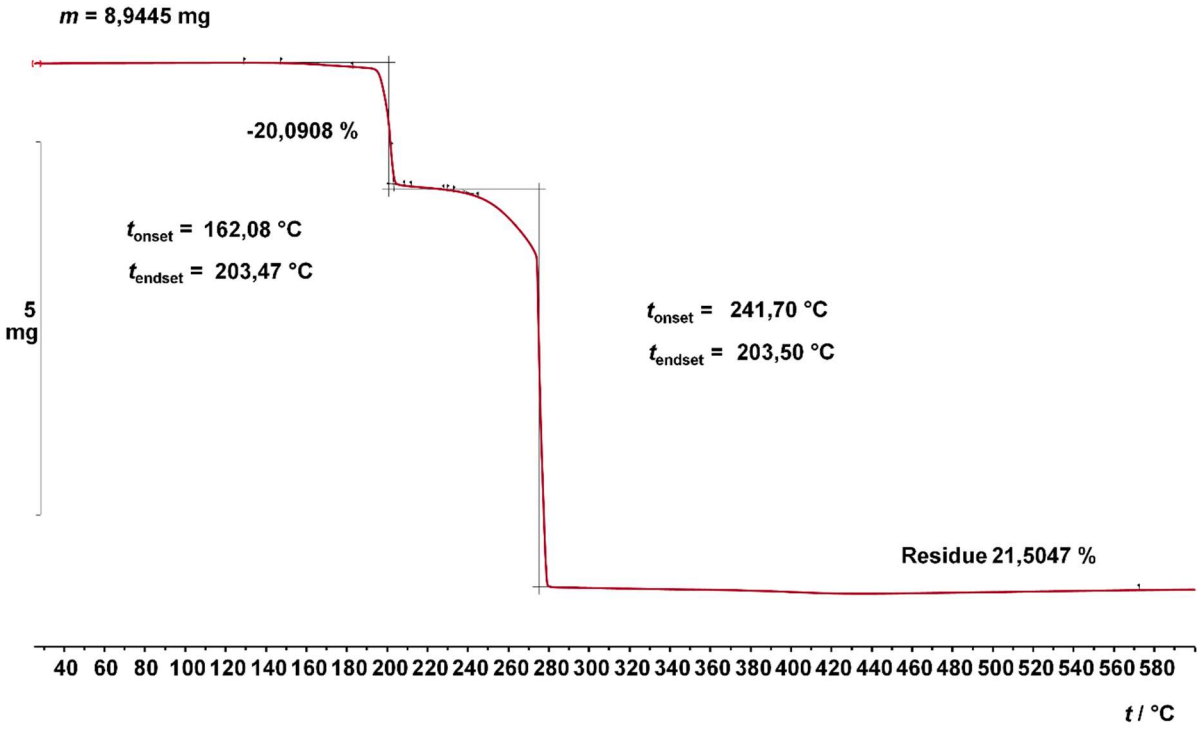

(a)

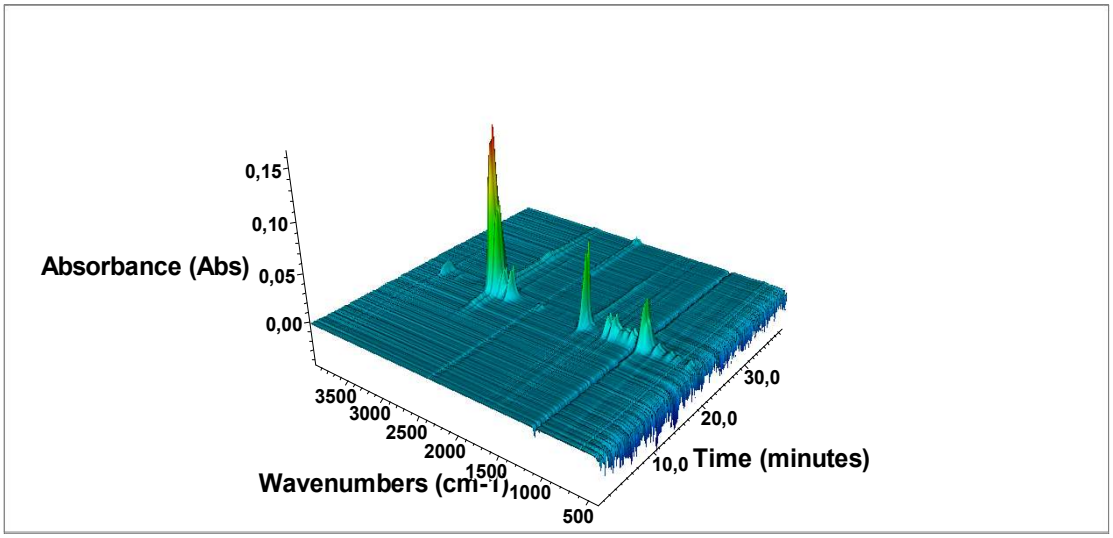

(b)

Fig. S21 (a) TGA curve of **1** under the O_2 atmosphere in the range of 25-600 °C (with a heating rate of 5 °C min^{-1}), (b) 3D FT-IR profile of the gas product evolved from **1** under the O_2 atmosphere in the range of 25-300 °C (with a heating rate of 10 °C min^{-1}).

2. Catalytic studies

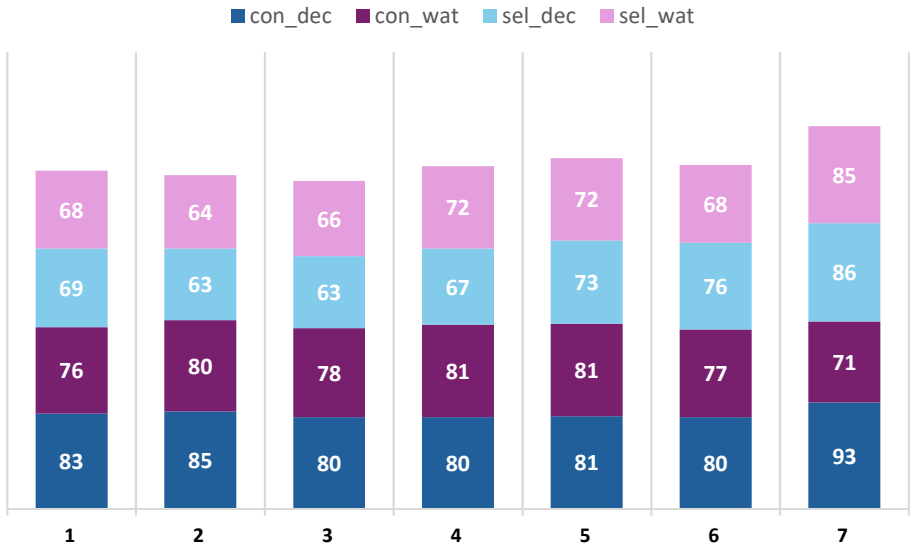

Fig. S22 Comparison of cyclooctene conversion and epoxide selectivity values for V catalysts **1**-**6** and Mo catalyst **7**, with TBHP in decane and water as an oxidizing agents.

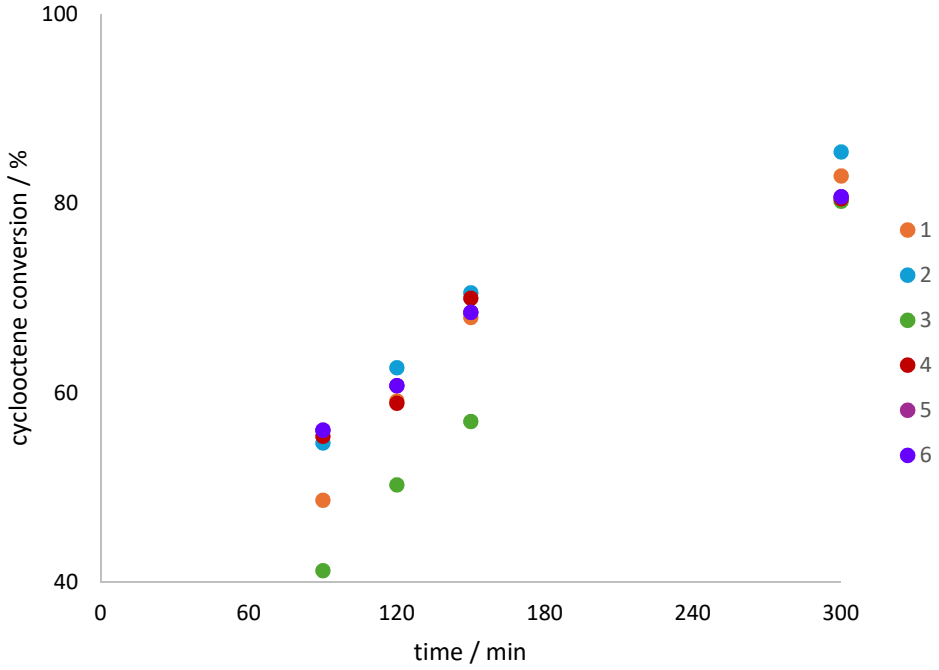

Fig. S23 Kinetic profiles of cyclooctene conversion with V catalysts **1**-**6**. The reaction temperature was 80 °C and TBHP in decane was used as an oxidizing agent. Reaction conditions: time, 5 h; temperature, 80 °C, *n*(catalyst)/*n*(cyclooctene)/*n*(oxidant) = 0.05 mmol/20 mmol/40 mmol.

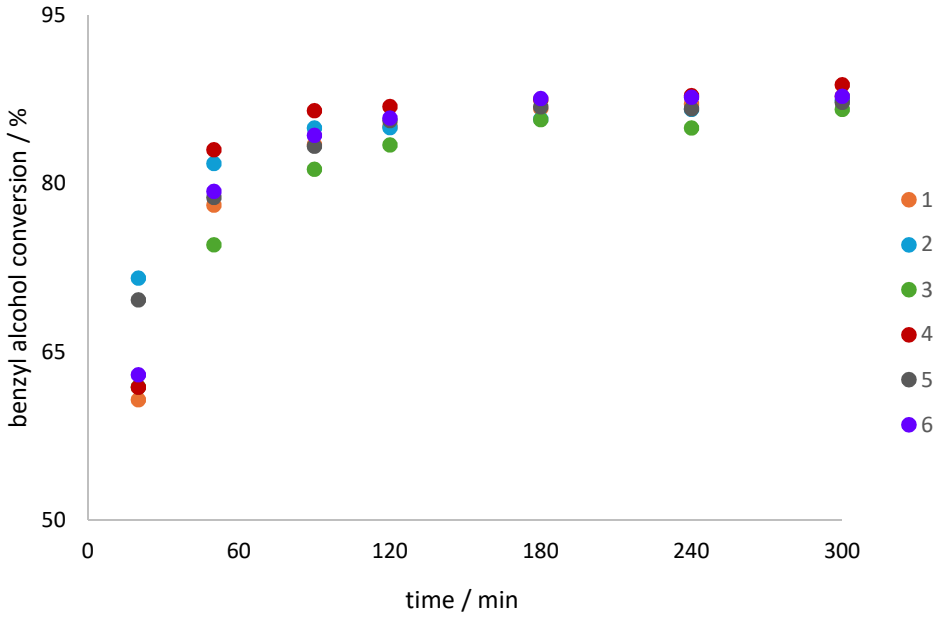

Fig. 24 Kinetic profiles of benzyl alcohol conversion with V catalysts **1**-**6**. The reaction temperature was 80 °C and TBHP in water was used as an oxidizing agent. Reaction conditions: time, 5 h; temperature, 80 °C, *n*(catalyst)/*n*(cyclooctene)/*n*(oxidant) = 0.1 mmol/20 mmol/40 mmol.

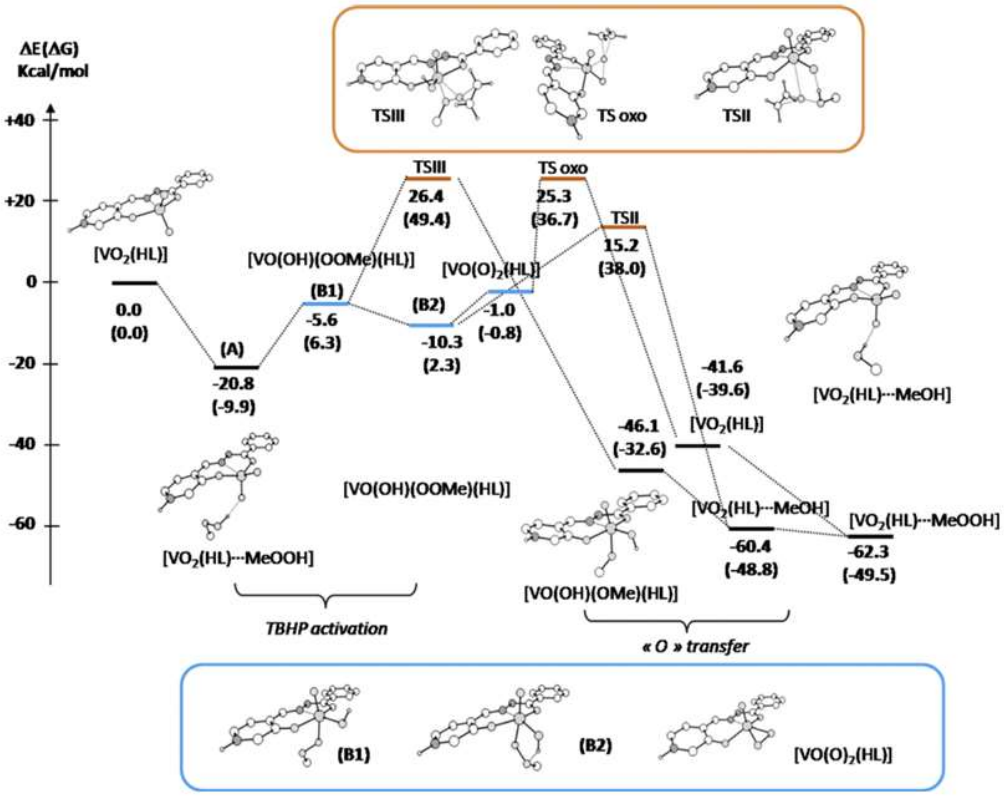

Fig. 25 Energy diagram of the epoxidation of ethylene by MeOOH catalysed by [VO_2(HL)] and views of the optimized structures (non-relevant hydrogen atoms were removed for clarity). The figure was taken from the reference 8.

Table S7 Catalytic results of benzyl alcohol oxidation. Reaction conditions: time, 5 h; temperature, 80 °C, *n*(catalyst)/*n*(cyclooctene)/*n*(oxidant) = 0.1 mmol/20 mmol/40 mmol

	Oxidant											
	TBHP in decane				TBHP in water				H_2O_2 with CH_3CN			
	Con[a] / %		Sel[b] / %		Con[a] / %		Sel[b] / %		Con[a] / %		Sel[b] / %	
	Reaction time / min											
Catalyst	300	20	300	20	300	20	300	20	50	20	50	20
[VO(acac)2]	72	22	37	71	87	55	14	47	29	33	38	36
V_2O_5	78	3	27	2	82	46	20	53	34	28	39	48

References

[1] T. Degen, M. Sadki, E. Bron, U. König, G. Nénert, G. The High Score suite. Powder Diffr. 2014, **29**, S13–S18.

[2] Rigaku Oxford Diffraction. CrysAlisPro Software System, Version 1.171.42.49; Rigaku Oxford Diffraction: Oxford, UK, 2020.

[3] G. M. Sheldrick, SHELXT– Integrated space-group and crystal-structure determination. *Acta Crystallogr. A Found. Adv.* 2015, **71**, 3–8.

[4] Sheldrick, G. M. Crystal structure refinement with SHELXL. *Acta Crystallogr. C Struct. Chem*. **2015**, 71, 3-8. doi:10.1107/s2053229614024218.

[5] O. V. Dolomanov, L. J. Bourhis, R. J. Gildea, J. A. K. Howard, Puschmann, H. OLEX2: a complete structure solution, refinement and analysis program. *J. Appl. Crystallogr.* 2009, **42**, 339–341.

[6] A. L. Spek, Structure validation in chemical crystallography. *Acta Crystallogr. D Biol. Crystallogr.* **2009**, 65, 148–155.

[7] C. R. Groom, I. J. Bruno, M. P. Lightfoot, S. C. Ward, The Cambridge Structural Database. *Acta Crystallogr. B Struct. Sci. Cryst. Eng. Mater.* **2016**, 72, 171–179.

[8] J. Pisk, J.–C. Daran, R. Poli and D. Agustin, Pyridoxal based ONS and ONO vanadium(V) complexes: Structural analysis and catalytic application in organic solvent free epoxidation*, J. Mol. Cat. A: Chem*., **2015**, 403, 52-63.